WPS 10th MSc Thesis, WPS10MSc

Renewable park control

Student number:	*Member:*
1# 20200641	Mikkel Lysgaard Poulsen

AALBORG UNIVERSITY
STUDENT REPORT

Supervisor(s):
Florin Iov
Alin Raducu

May 30, 2022

Aalborg University

Department of Energy and Technology

AALBORG UNIVERSITY
DENMARK

AALBORG UNIVERSITY
STUDENT REPORT

Department of Energy and Technology
Aalborg University
http://www.aau.dk

Title:
Renewable park control

Theme:
Scientific Theme

Project Period:
Spring Semester 2022

Project Group:
WPS4 - 1051

Participant(s):
Mikkel Lysgaard Poulsen

Supervisor(s):
Florin Iov
Alin Raducu

Copies: 1

Page Numbers: 57

Date of Completion:
May 30, 2022

Abstract:

In the transition towards renewable energy production, there has been an increasing tendency to incorporate additional storage into the power plants. This project deals with the design and tuning of a renewable park controller and the main focus has been on active power and frequency control. A hybrid power plant including wind turbines, PVs, and a power to hydrogen plant rated 60 MW including a 10 MW of hydrogen production has been implemented to verify the functionalities of the controller. The requirements for the controller are based on the danish grid codes. A PI controller has been developed for the hybrid power plant. The controller has been tested under different operational conditions to verify the robustness and the capability of rejections due to disturbances in the system. Two dispatch strategies have been investigated to maximize the available power in the system. One is based on proportional dispatch and the second is based on minimizing mechanical stresses in the wind turbines. The discretization method is investigated to find the optimal solution for implementing the controller in a real-life environment in order to avoid disturbances under production. The controller is tested under steady-state conditions to verify the controller according to the grid codes.

Preface

This report has been conducted as a result of a Master's Thesis at Aalborg University. The project group WPS-1051 consists of members from Wind Power System at the department of Energy Technology. The project has been created based on an interest towards a CO_2 free future. The thesis is investigating the challenges when implementing PtH in combination with renewable energy sources.

Reading Guide

The knowledge for the report is conducted based on literature from articles, books, web-pages and standards. The sources used for the report is cited and found in the bibliography. Figure and table are numbered according to the respective chapter. Figures and table without reference are developed by the report writers. Furthermore, graphs used for the report are developed in MATLAB.

Mikkel Lysgaard Poulsen

Summary

Når Danmark i 2050 skal være C02 neutral, skal nye og innovative løsninger være med til at nå målsætningen. Dette skal gøres gennem vedvarende energiproduktion, hvor forskellige typer teknologier skal sammensættes (herunder windmøller, solceller og elektrolyseanlæg). Rapporten omhandler styring af den aktive effekt produceret af anlægget, og hvordan den aktive effekt udnyttes bedst muligt af enhederne. Motivationen for dette projekt er beskrevet i kapitel 1, hvor også problemformuleringen og begrænsningerne findes. De nyeste teknologier bliver beskrevet i kapitel 2, hvor litteratur om regulering og styring af vedvarende energiparker beskrives. Reguleringen for eksisterende anlæg bliver lavet med en PI regulator, hvor den aktive effekt måles i PCC og sender værdierne tilbage til regulatoren. I kapitel 3 beskrives modelopbygningen af systemet. For at udarbejde en belastningsanalyse ved hjælp af Power System toolbox, bliver distributionsnettet repræsenteret af en Thevenin ækvivalent. Thevenin ækvivalentes parametre som SCR og XR-værdier estimeres ud fra antagelsen om tilslutning til et stærkt og stabilt distributionsnet. Ydermere bliver kablerne for modellen repræsenteres af en π-model. For at simplificere netværksmodellen anvendes første ordens overføringsfunktioner som repræsentation for produktionsenhederne. Dettes gøres for, at klassisk reguleringsteori kan anvendes i regulatoren. Resultaterne af belastningsanalysen beskrives i kapitel 4, hvor indvirkningen af netværkstilslutningen undersøges. Analysens resultater anvendes til at estimerer den tabte aktive effekt mellem produktionsenhederne og net tilslutningen. På baggrund af denne estimering designes en regulator i kapitel 5, som tager højde for tabet i netværket. Regulatorens modstand overfor netværksforstyrrelser testes og valideres i forhold til de tekniske forskrifter for net tilsluttet vindmølle- og solcelleparker. Regulatoren implementeres derefter i z-domænet og valideres jævnfør kravene fra de tekniske forskrifter om net tilslutning.

Nomenclature

Abbreviation	Definition
AWE	Alkaline water electrolysis
BOP	Balance of plant
HPP	Hybrid power plant
PCC	Point of common coupling
POC	Point of connection
PV	Photovoltaic
RES	Renewable energy sources
RPC	Renewable park controller
TSO	Transmission system operator
WPP	Wind power plant
WT	Wind turbine

Table of contents

List of Figures

List of Tables

1 Chapter 1: Introduction

1.1 Back ground for the hybrid power plant controller

In 2020 Denmark began a new adventure within the transition towards a CO_2 reduction of 70 % in 2030 and become 100 % CO_2 neutral in 2050. With a strong position in offshore wind energy and home place for some of the largest wind energy companies in the world, Denmark is one of the top leaders towards a CO_2 free future [1] [2]. To reach the goal of a CO_2 free future, a huge investment in carbon capture and electrolysis plants is presented from the Danish government in the *climate agreement* from 2020. To accelerate the technology, a fund of 750 Mio. DKK is created to secure the development of PtX projects for the non-electric sector. Long-term analysis from Energinet shows that Denmark is in a strong position for commissioning PtX plants. The excess renewable energy production can be converted into hydrogen via electrolysis. By further processing, the hydrogen can be converted into gaseous and liquid fuels. From the analysis, it is also expected that the PtX technology can compete against fossil fuel alternatives in Denmark by 2035 [3]. To counter the increasing energy demand in Denmark, the construction of two energy islands with a total capacity of 5 GW wind power are planned to be placed in the North Sea and the Baltic Sea respectively. By the completion of the energy island in the North Sea, the total capacity from the plant is expected to be 3 GW but can be extended to 10 GW [4]. Depending on the demand in the future, the next phase of the island is to implement energy storage and PtX.
PtX is a part of the solution to lower the CO_2 emission in the future. This is seen at Hanstholm Harbor, where the vision of the harbor is to become the first CO_2 neutral fishing harbor. The harbor is installing wind turbines and solar panels in an off-grid system to produce e-methanol for their fishing boats [5]. Furthermore, an increasing trend is seen from the plant operators for implementing photovoltaic (PV) and batteries in already existing onshore wind power plants (WPP). By implementing the new generation in already existing plants, new development of the infrastructure is avoided. An important challenge for the expansion of such a plant is to avoid overload at the point of common coupling (PCC) due to the extra generation and storage units. To overcome such challenges a suitable controller for the park must be implemented to ensure a stable operation for the plant. Since the share of hybrid power plants (HPP) is increasing is it important to understand the impact and contribution of such technology connected to the grid. Moreover, to investigate the effect on grid stability when the future electricity production is based on HPP production [6]. All mentioned HPPs are based on wind turbine production combined with storage or another RES technology. From the literature, [7] and [8] the reactive power and voltage control research is well described and documented. On the other hand, the impact of active power from the RES is more challenging due to the direct impact on the frequency stability [9]. Studies from the first utility scaled HPP [6] show the potential of utilizing the surplus energy production instead of curtailing the RES to meet the reference setpoint at PCC.

In Figure 1.1 different types of HPP is shown. It is seen that wind turbines in combination with PVs are sending the produced electricity to an electrolysis plant or directly to the grid. The layout of such plants can both be onsite or off-grid, like the energy island and Hanstholm Harbor, respectively. The figure shows two possible layout solutions for the HPP design but a large number of different selections can be achieved. The electrolysis plant is placed behind the grid meter and is mostly supplied by the HPP itself. It is expected that the plant is able to deliver 50-80 % of the PtX plant electrical consumption [3].

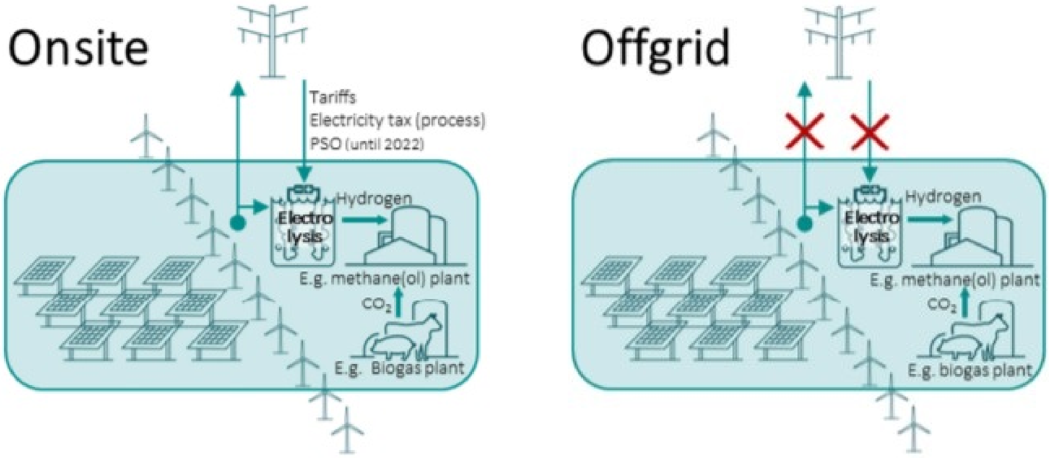

Figure 1.1: Types of constellations for HPP [3].

A hybrid power plant (HPP) consists of multiple production units and to maximize the plant production, a controller for the HPP is implemented. The purpose of the controller, which is called a renewable park controller (RPC), is to coordinate the control of the HPP and to comply with the national grid codes.

In Figure 1.2 a typical overview of the hybrid power plant controller layout is illustrated. The plant is treated as a single generator unit, similar to a conventional power plant with one PCC. A setpoint sent from the plant operator or the transmission system operator (TSO) is received in the RPC and based on a hierarchical structure, it is distributed further to the production units. For a HPP connected to the medium voltage range, the setpoint in sent from the DSO.

The signals sent to the units (WPP, PVP, etc.) is then treated internally by a controller, which is usually provided by the manufacturer of the specific plant.
The RPC has to ensure that the HPP is complying with the grid codes. To ensure this, communication infrastructure is placed between the PCC, RPC, and the production units, where different signals of measurements and setpoints are exchanged.

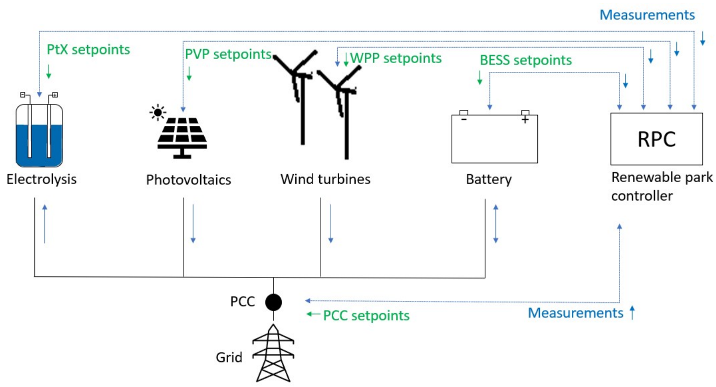

Figure 1.2: Overview of a typical plant control architecture. Inspired by [10]

To operate an HPP the renewable park controller must be aware of the different dynamics of the units in the park. For the specific plant (WF, PVP, etc.) specific grid codes and reaction times for control are applicable. In the technical regulation 3.2.5 for a wind park larger than 11 kW in Denmark, the plant must respond on a new active power setpoint no later than 2 seconds and complete the control no later than 10 seconds [11]. The same applies for a PVP larger than 11 kW in Denmark (technical regulation 3.2.2) [12]. The PVP must respond within 2 seconds and complete no later than 10 seconds for a new active power setpoint according and the same applies to the battery. However, to regulate active power, the RPC needs to control the state of charge for the battery, in order to curtail or inject active power to the grid. To absorb active power in case of over-production compared to demand, a control for the battery must ensure that the state of charge for the battery is not exceeding a certain setpoint [13]. In the case of a fully charged battery, a PtX plant could be implemented to further utilize excess power production. The dynamic of the PtX plant might be different compared to the other units and a combination between the PtX and battery are likely. Despite the same time response for regulation, the time response for the individual plant might be different due to the dynamics of the units (power electronic, mechanical limitation, etc.). Therefore, the RPC must be able to distinguish between the plant units/modules, where the units with a fast response time are used for transient disturbances and replaced by units with slower response times, but larger capacity in case of longer periods.

1.2 Ancillary services

To ensure a stable power system, consumption and demand must be kept in balance. Changes in demand or disturbances in the grid can lead to frequency deviations, which can have an impact on the units connected to the grid. To keep the power system in balance the TSO of Denmark *Energinet* buys ancillary services from the power plants. Thereby, the power system is kept as reliable and stable as possible. However, these services can not be provided by WTs and PVs. The following ancillary services provided in DK1 are listed:

- Primary reserve, FCR
- aFRR supply capability
- Secondary reserve, aFRR
- Manual reserves, mFRR
- Properties required to maintain power system stability.

Under normal operation, the HPP is delivering absolute power production or limited production based on the setpoint sent to the RPC. However, the plant owners can increase the revenue by offering additional ancillary services for the TSO [14]. In case the HPP must curtail the production due to the services implementation of a storage system to absorb and utilize the available power in the plant is a feasible solution. Furthermore, when the energy is needed in the grid, the electricity is then sent to the PCC and the electricity to the storage or PtX is decreased.

Depending on the ancillary service, different requirements are made. Energinet is buying primary reserve 6 times a day and this service is therefore well suited for all units in the HPP, due to a well forecast and estimation of available power for the plant. However, for aFFR, the services are bought for a whole month, which is why RES might not be a feasible solution for such services due to unpredictable forecasts. Therefore, a production unit as a battery and a PtH (which is considered as a load) could be a feasible solution due to their non-reliable on the weather. For primary reserve half of the reserve must be injected into the system no later than 15 seconds and fully delivered within 30 seconds. The injected reserve must be fully recovered within 15 minutes. However, according to[14] wind power plant and solar panels are not allow to bit on this market without other types of generation to guarantee supply due to failing sun/wind resources. To recover the primary reserve, the secondary reserve is activated and should be fully injected into the system within 5 minutes and the rated capacity is usually $\pm$ 12 MW. Based on the longer response time for the services compared to the grid code, a device with a higher black start time could be feasible to offer for such a service. A PtH plant is one solution, where the operator is paid for curtailing the power and paid for the produced hydrogen. This is only suitable if curtailing of the active power is needed and for an increase in the power, a battery could then be used. For an HPP to participate in such an operational mode, the RPC must be advanced enough to distinguish between the services, which the different plants are providing. Therefore, it is needed to investigate dispatch strategies, limitations of the different plants, and the needed capacity.

In the hybrid power plant that is to be connected to the grid to provide specific grid services and maximize revenue, it is crucial for the plant to absorb excess power production. Due to a varying production profile from the renewable energy sources, the available power from the HPP can be higher than the power needed at the PCC. To make use of the excess power from the plant, a device that can absorb power when needed or turned off in case of deficit in power production. When opting for such a solution it is necessary to investigate feasible products on the market which can comply with the dynamic of the HPP. For the proposed system an A90 electrolyser provided by *Green Hydrogen Systems* is chosen. The advantages of the A90 is that the stack is easily scalable with a low cost and high efficiency. The specifications for the hydrogen plant is based on the data sheet [15].

1.3 Problem Statement

This project is carried out in a collaboration with Vattenfall A/S, which is building and operating renewable and hybrid power plants. For an HPP several renewable technologies are combined into one production unit. When a wind power plant, PV plant, or storage is acquired, the manufacturers are typically providing the production units and the software as one combined product. The control operator at the hybrid power plant needs the knowledge of how to control the plant and how to adjust it by various parameters. This must be acquired for a large number of HPP combinations, containing different plant designs. Furthermore, based on the dynamics and the response time of each plant inside the HPP, it is required by the RPC to dispatch the correct setpoint for each unit/module, which includes an electrolysis plant. Based on the location of an HPP, the plant needs to fulfill the control functions required at the certain place. Furthermore, the dispatch should be optimized to maximize energy consumption from the hybrid power plant.

1.4 Objective

The previously outlined challenges lead to the following objectives that are desired to be achieved for this project.

- Dispatch strategies that increases energy capture while reducing operational costs
- Coordinated control of active power and frequency control according to specific grid code requirements
- Verify robustness of the RPC through simulation studies

1.5 Methodology

To make the project succeed, several methods has been utilized trough the project. An analytical approached has been taken in order to identify the main challenges for the HPP consisting of large penetration of renewables energy sources. To investigate feasible applications for a HPP including an electrolysis plant, the public domain has been browsed.

To investigate the power flow in the system Newton-Raphson method has been utilized in order to investigate the steady state conditions for the HPP. The hybrid power plant is developed in Matlab Simulink.

1.6 Limitations

Due to the large scope of the project it has been necessary to form some limitations for the project. Therefore, the project only deals with active power control and the limitation for the project are stated:

- The controller for the hybrid power plant will only consist of active power control.
- The system is considered as balanced and the control will be made under normal operation.
- The system does not include investigation of short circuit event during operation.

- Harmonics and disturbances due to voltage source converters from the production units is not investigated.

2 Chapter 2: State of the art

2.1 Introduction

In this section, an overview of renewable park control is presented. The control strategies related to the topic is investigated and discussed. An overview of a common dispatch strategy is described, where the advantages and disadvantages are discussed related to RPC. Furthermore, commercial Power to Hydrogen plants is investigated in order to find the technical specifications for the plant operation.

2.2 Renewable park controller (RPC)

For a HPP which consists of multiple production units/modules a software is needed to control all the aspects of the park. A method to approach this, is by implementing a renewable park controller. In Figure 2.1 an illustration of a RPC is shown [6]. The RPC includes a controller and a dispatcher. The principle is that the controller is regulation the total production in the plant at PCC. The controller is then sending a setpoint to the dispatch, which is calculating the correct setpoint for each module in the HPP. In order to compute the signal for each module, the controller is receiving inputs signals from the plant. This includes production capability from each unit, measurements at PCC and control inputs from the plant operator.

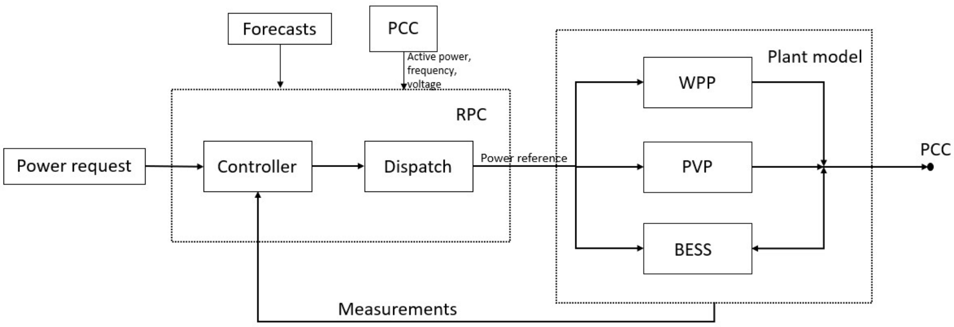

Figure 2.1: Illustration of RPC. Inspired by [6].

To ensure the correct amount of power in the PCC, that is requested by the operator or the TSO, a controller is implemented to eliminate any deviation between the input signal and the output signal. The deviation or the incorrect power received in the PCC is caused due to the cable losses, when the power is send from the production units to the PCC. The paper [6] is proposing a PI (proportional integral) controller to ensure stable and accurate delivery to the PCC. The PI controller is a simple method to control a given setpoint and is well known, and used for other power plants, as mentioned in [16]. The controller in the RPC must be advanced enough to control multiple production units, with different dynamics under performance. Furthermore, by using the PI controller it is easily to scale the system due to the simplicity of the method. From the business case perspective presented by [6], where additional production modules is added to exciting plants, the PI controller is well suited for a RPC. The advantages of the RCP is the simplicity of the control. The RPC is scalable and easy to implement in new systems. However, the RPC does not include a power to hydrogen module and therefore further research is needed in the area.

2.2.1 control structure

In Figure 2.2 a control structure of the renewable park is shown [17].

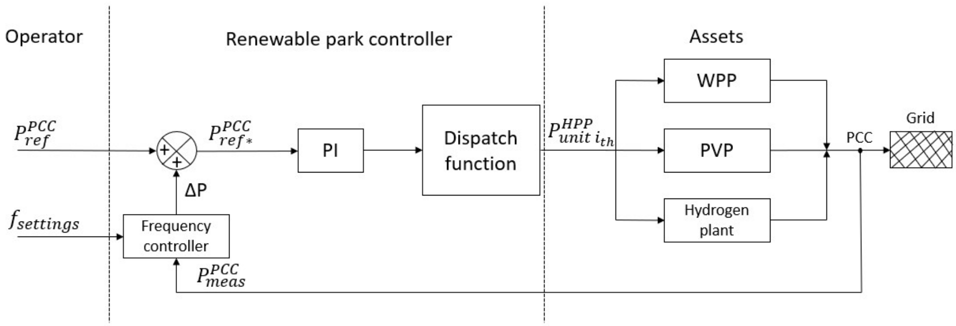

Figure 2.2: Control structure of renewable park. Inspired by [17].

In normal operations a setpoint is sent from the operator P_{ref}^{PCC} to the renewable park controller as a generation reference to the PCC. Depending on the settings from the frequency controller ΔP an adjustment for the generation reference can be made and gives a new reference P_{ref*}^{PCC}. In the diagram it is expected that the power factor at the PCC i unity and therefore the reactive power setpoint is neglected. In case of reactive power adjustment, this can be achieved either by the grid site of the PCC or by a STATCOM. The error between the requested power P_{ref}^{PCC} and ΔP is treated in a PI controller in order to eliminate the error. The corrected setpoint is then sent to the dispatch in the RPC, which is distributing the individual setpoints $P_{unit\ i_{th}}^{HPP}$ for the generation units in the plant. The power is sent to the grid where a grid meter is measuring the power at the PCC. This is sent back to the frequency controller and a new P_{ref*}^{PCC} is sent to the RPC.

2.2.2 Unit commitment for hybrid power plant

For the hybrid power plant it is important to maximize the power production and minimize the operational cost. The operational production cost for a hybrid power plant based on RES, is mainly for maintenance since no fuel is acquired for the operation of the plant. A common method used for the plant operators to meet the power demand by regulation the operational conditions is known as unit commitment (UC). UC is a method to scheduling the generator units by taken three main keys in to consideration. By considering the availability of power, operating system stability and economical production costs, the UC method is able to scheduling the generator units in the HPP. The objective for the scheduling is to keep the power balance at the requested amount and still be able to fulfill the constraints set for the system (generator power output limits, spinning reserves, limits of ramp rate, and minimum up/down time)[18]. From the literature [19] a proposed method based on wind energy production and thermal production is used. The principle of distinguishing between the generator units is similar to the HPP, however some few adjustment might be necessary in order to adapt this to the HPP.

To create the most efficient and economical dispatch using unit commitment, is by developing an objective function, that is based on the amount of power production and the cost for each unit. To describe the dynamic of the plant, several constraints is developed, such as power balance, spinning reserve, ramping up/down speed, unit generation limits, etc. The power balance constraint is to ensure that a balance between production and consumption is equal. To prevent a deviation of active power in the system a constraint for the spinning reserve is developed. This is to ensure that, a minimum amount of active power is kept in reserve. Due to the limitations of the ramping capacity between the different units, ramping up/down constraints is developed for each unit. The advantages of unit commitment is to utilize all the different modules in the HPP in the most optimal way. This is based on a optimization algorithm, where the dynamic of the system is implemented. However, the disadvantages for the the unit commitment is the complex optimization algorithm. The algorithm require a large amount of computer power and the advantages gained from the unit commitment can maybe be achieved by a simpler system.

2.2.3 Power to hydrogen

As a the market for hydrogen production from renewable energy sources is growing, various companies are providing such solution. In order to find relevant material for further usage, different companies is investigated for the technical descriptions. Companies as *Greenhydrogen* and *HyBalance* are both providing solutions for power to hydrogen production which is available on the market at the moment. From available data in [15] and [20] technical parameters from the plants are provided in Table 2.1.

Table 2.1: Technical parameters from power to heat plants.

Stack size	450	kW
Efficiency	76.2	%
Ramp-up time	10	s
Ramp-down time	10	s

2.3 Summary

The state of the art of renewable park control has been presented. It is seen from the scientific literature that the main regulator for RPC is a PI-controller which is why this is chosen for the project too. Furthermore, modern dispatch optimization strategies is investigated, where a further development of such control is to be made. This is due the disadvantages related to maximising power production based in optimization and the complexity of such solution. Moreover, several power to hydrogen companies has been found in order to investigate the possibilities of implementing of such solution. The technical specification for the plant has been collected for further usages.

3 Chapter 3: System characterization and network modelling

3.1 Introduction

The performance of the renewable park controller is based on an already existing renewable park. The renewable park is located in Haringvliet, where the park is including a WPP, PVP, and a BESS. For his project, the BESS is neglected and an electrolysis plant is implemented instead. The plant consists of 6 wind turbines rated 3.6 MW (22 MW total), and 115.000 solar panels rated 38 MW in total. Thereby, the total peak production of renewable is 60 MW. The wind turbines and the solar panels are treated as one production unit respectively, and is connected in the POC (point of connection) as seen in Figure 3.1. The WPP and PVP are expected to deliver a unity power factor at the POC and the RPC is to control the power output at PCC. The HPP is located onshore, which means that the PCC is connected at the distribution voltage level. The distribution voltage is determined to be 60 KV. The power to hydrogen plant is rated 10 MW based on the existing project from *REFHYNE* in Germany [21].

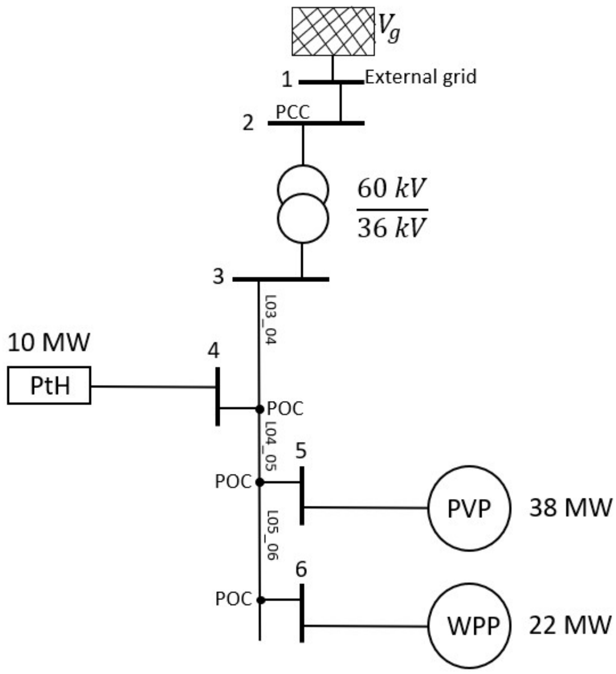

Figure 3.1: Single line diagram of a renewable park [22].

The distribution network is managed by the DSO and from the technical regulations 3.2.2 [12] and 3.2.5 [11], a maximum and minimum voltage range are to be expected at the PCC. However, the parameters from the external grid (SCR and XR ratio) are unknown and an approximation for these is to be made. By representing the external grid (V_g) with a Thevenin equivalent which includes the grid voltage, SCR, and XR ratio the behavior of the external grid can be estimated. Moreover, the characteristic of the underground cables must be determined for further development of the single line diagram.

3.2 External grid representation

A method to obtain the dynamic at the point of common coupling is necessary in order to investigate the impact of the grid on the plant. A method to approach this is described in the literature [23], where the external grid is represented by a voltage source (V_g) behind a grid impedance (Z_g), this is shown in Figure 3.2. The voltage source V_g and the impedance Z_g is representing the entire grid connected to the power plant.

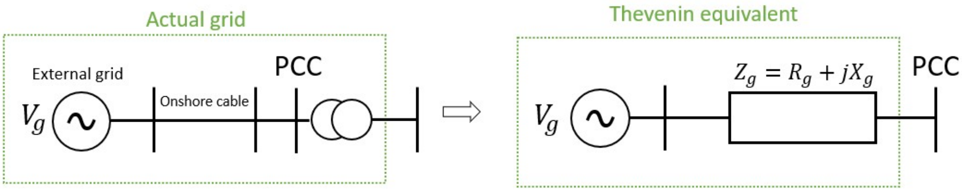

Figure 3.2: Thevenin equivalent for the representation of the entire external grid to the HV/MV transformer [23].

From Figure 3.2 the representation of the external grid is shown. The representation of the external grid is to capture the dynamics of the entire grid to the HV/MV transformer. The Thevenin equivalent is based on the voltage at the PCC, an appropriate short circuit ratio, and XR ratio. The SCR is defined by the short circuit power (S_k) and the rated power from the plant at PCC (P_{rated}^{PCC}). This is defined as:

$$SCR = \frac{S_k}{P_{rated}^{PCC}} \tag{1}$$

By using the grid voltage (V_g) and the short circuit power (S_k) the grid impedance (Z_g) is denoted by:

$$Z_g = \frac{V_g^2}{S_k} \tag{2}$$

From the grid impedance (Z_g) and the XR ratio, the resistance and inductance of the system are found by the equations:

$$R_g = \frac{|Z_g|}{\sqrt{1 + XR^2}} \quad \wedge \quad X_g = R_g XR \tag{3}$$

By choosing an appropriate SCR and X/R ratio, the grid impedance can be derived for further development.

3.3 Wind power plant model

With a large number of wind turbine manufacturers and models which can be installed onshore a general approach for the WT is needed. This is to simulate the impact of the wind turbines connected to the network. The model must be simple enough to represent the system, but also advanced enough to capture the dynamics of the system. Due to the time frame, the model is not designed to capture the fast variations in the wind speed and the electrical components inside the WT (transformer, power electronic, etc.). Therefore, a simplified model has been taken into consideration, which is based on the performance of the power output [24]. To simulate the performance of an actual wind farm, a modified wind turbine model proposed in [25] is been taking into consideration. Furthermore, the same model has been proposed in [26] with an additional ramp rate limiter and a power limiter added. The proposed wind turbine model is shown in Figure 3.3.

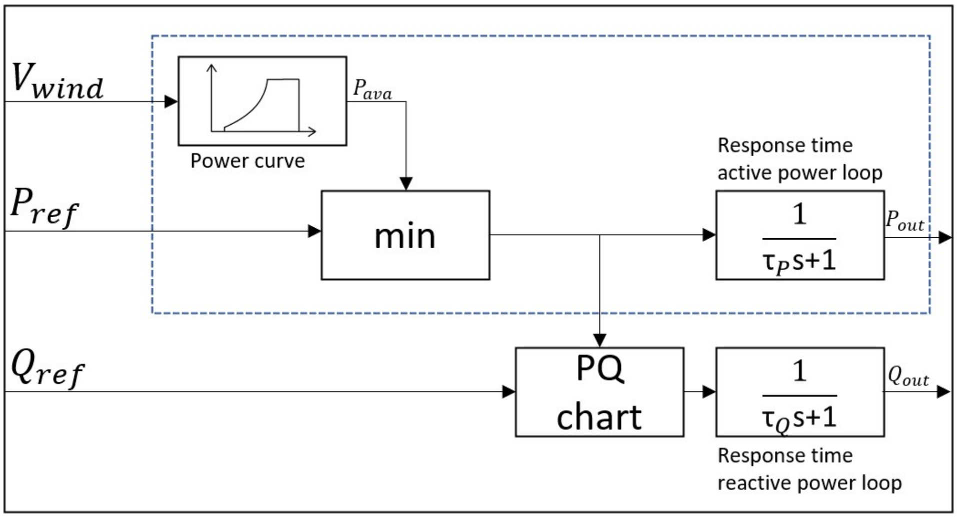

Figure 3.3: Block diagram of the proposed wind turbine model[26].

In Figure 3.3 a block diagram of a wind turbine is shown. The figure consists of 3 inputs (wind speed (V), active power setpoint P_{ref} and reactive power setpoint Q_{ref}). The setpoint is mostly set by the plant operators to increase or decrease power production. This is shown as the two power outputs P_{WTout} and Q_{WTout}. The majority of modern wind turbines on the MW scale are based on either a Type III (double fed induction generator) or a Type IV (full-scale converter). The Type III, DFIG is capable of both delivering active and reactive power. However, the reactive power is dependent on the active power produced by the WT [27] [28]. A typical range for the reactive power is between 25-30 % of nominal power. For the Type IV full-scale converter, the active power is produced by the converter, and the reactive power produced is fixed. To compensate for the power losses from the WT to the PoC a P/Q chart is implemented. The losses are caused by the generator and converters inside the WT (Figure 3.3). The wind turbine model for the system is based on a Vestas V112-3.0 rated 3 MW [29]. To ensure a stable operation and to protect the wind turbine from high wind speed, the WT is capable of pitching in and out in the range of 3 m/s to 25 m/s.

The active and reactive power loops are treated as first-order systems, with a time constant of τ_p and τ_q respectively. A typical time constant for the τ_p is approximately 1 s and a typical time constant for the τ_q is approximately 0.2 s [30] [26]. Furthermore, the limits for the maximum allowed change in P_{ref} from [29] is 300 kW/s, which corresponds to 0.1 p.u/s.

3.4 PV model

For the PVs, a various amount of diffent type exist on the market today. From the literature, [31] different types of layout is shown, where a large-scale PV plant is connected to the distribution grid. Therefore, a general approach for a PV is to be developed. The dynamic of the model must be simple to represent the system, but advanced enough to capture the performance. Therefore, transformer and electrical devices are neglected, and the model is seen in Figure 3.4. The model of the PV is based on [25]. A similar model has been proposed in [32], to conduct the dynamics of the PV plant.

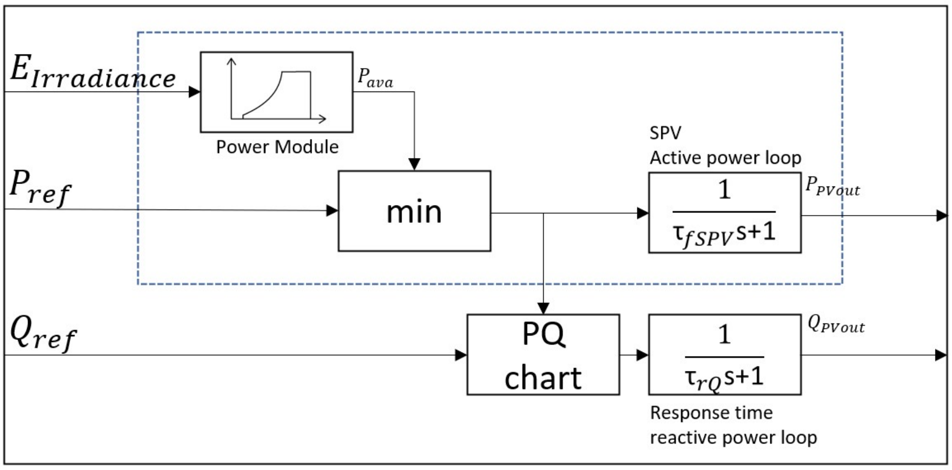

Figure 3.4: Block diagram of the proposed PV model[25] [32].

In Figure 3.4 a block diagram of the proposed PV model is shown. The figure consists of three input and two output signals. The signal $E_{irradiance}$ is the input for the power module and the power output from the model is the available power from the plant. P_{ref} and Q_{ref} is determined by the plant operator, where setpoints are sent to the plant. The power production from the plant is seen as P_{PVout} and Q_{PVout}, which is depending on the input setpoints. A PQ chart block is implemented in the PV model to compensate for the losses between the PV modules and the PoC. The PV model is represented as a first-order transfer function, where a time constant is representing the dynamics of the system. Appropriate values for the time constant in the PV model are approximately 1 s for the active power and 0.2 s for the reactive power [26]. According to [30] a appropriate ramping limit for the PV is 20 p.u/s.

3.5 Power to hydrogen model

With limited research on utility-scaled Power to Hydrogen plants combined with multiple WTs and PVs connected to the same PCC, an approximation of the PtH model must be taken into consideration. The PtH plant is to be considered as a load, which consumes excess active power from the WTs and the PVs when the demand is lower than the available power in the HPP.

Despite the electrolysis plant being seen as a load, a performance model of the plant must be developed in order to capture the dynamics of the load.

In order to develop a suitable simulation model for a PtH plant, some approximations have to be taken into consideration. From [33] a test for secondary control has been made. The power consumption from the PEM plant is shown in the article and a representation of the test can be made by a first-order transfer function.

The stack is expected to have two inputs, one for the active power consumption and an input signal for the power reference. The output of the plant is the so-called "X", which is hydrogen for this plant. The performance model of the stack is to cover the overall performance of the unit and does not cover the dynamics of the components inside the plant (electrical parts, etc.). The stack unit is therefore treated as a first-order transfer function with an appropriate time constant to capture the dynamics inside the stack. From [20] the manufacturer provides a response time of 10 s. This is also seen from [33] where the time response is approximately 15 s. From [33] the ramp rate limits for a PEM utility-scale plant were found to be approximately 0.05-0.1 p.u/sec. Due to the rated capacity of the stack, a power limiter block is implemented. The total efficiency for the electrolyser stack is 76 % [15]. This is due to the losses in the power conversion from AC to DC and the efficiency of the stack itself. A representation of the electrolysis stack is seen in Figure 3.5.

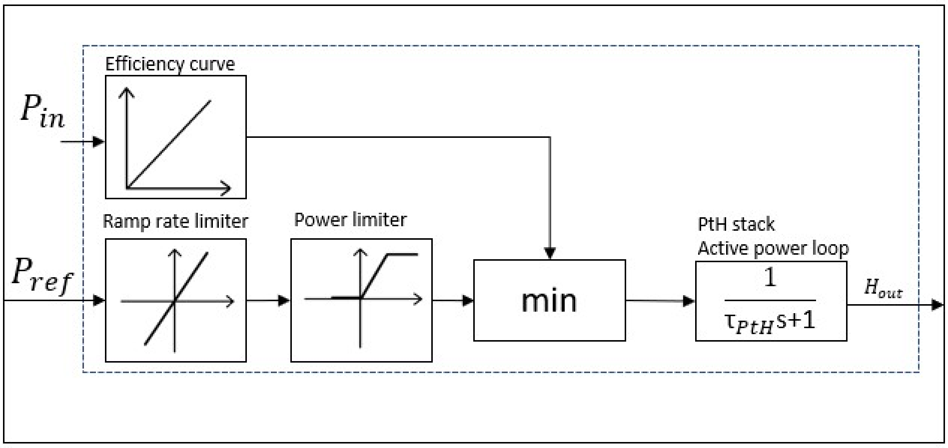

Figure 3.5: Block diagram of the proposed PtH stack model. Modified and inspiration based on [25] [26].

The stack is seen as a load and consumes excess active power from the HPP. Due to a long black start time found in [34] the electrolysis stack is assumed to be in operation mode and does not need any startup time to consume active power. However, an appropriate time constant for the transfer function is assumed to be 2.5 sec based on [20]. An appropriate size for the maximum stack power consumption is assumed to be 450 kW according to [15].

3.6 Modelling of the lines

From the Figure 3.6 a π model is shown. The model is a theoretical representation of the underground cable and overhead lines. The line representation includes a series resistance (R), inductance (X), and half of the shunt admittance (Y). One part of the admittance is lumped at the sending side, while the other half is lumped at the receiving end. By considering half of the admittance for both the sending and receiving side the line viewed from both ends is the same. This model is used for a medium length line, which is considered for the proposed HPP. The line representation is used for the load flow analysis and the model is well suited for load flow analyses and dynamic system stability studies [35].

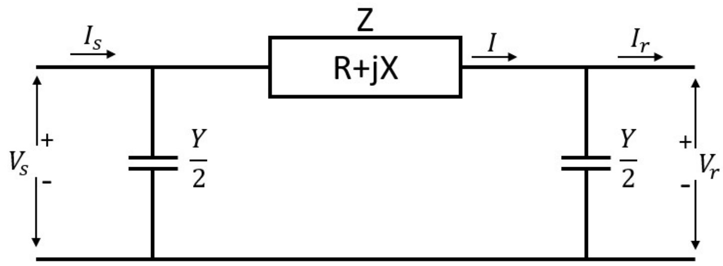

Figure 3.6: Line representation by the π model [36].

Values in the line model are usually represented per unit length and the shunt admittance from Figure 3.6 is expressed by the following notation.

$$Y = j \cdot \omega \cdot C \tag{4}$$

4 Chapter 4: Model validation and plant design

To verify the proposed line model for the hybrid power plant the model is implemented in the software Power System Toolbox in Matlab [35]. The toolbox is seen as a reliable method to obtain the steady state conditions for the plant. The test is based on the Newton-Raphson method and the parameters are from the single line diagram in Figure 3.1. The purpose of the load flow analysis is to investigate the losses in the network for further development of the controller. The load flow studies calculate the magnitudes and angle of the voltages phasors. These values are used to determine the losses in the network, and described by the following equation:

$$I = Y_{bus} \cdot V \tag{5}$$

where I is the N_{th} vector of source currents injected into each bus. V is the N_{th} vector of bus voltages and Y_{bus} is the admittance matrix for the network [36].

The injected current to the system is determined by the known active and reactive power, and is denoted as followed

$$I_k = \frac{P_k - Q_k}{V_k} \tag{6}$$

where P_k and Q_k is the injected active and reactive power into the N_{th} busses respectively [36].

The impedance between the sending and receiving end is illustrated in Figure 4.1

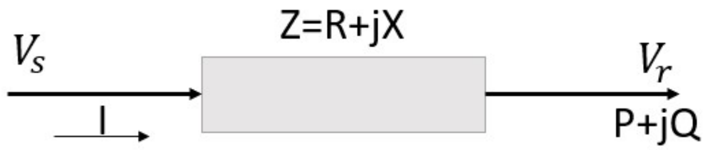

Figure 4.1: Voltage drop along line. Inspiration found from [37].

The voltage drop at the sending end is the found as followed.

$$V_s = V_r + ZI = V_r + (R + jX)(\frac{P - jQ}{V_r}) \tag{7}$$

From the known bus voltages and line currents, the power losses in the system can be calculated. This is achieved by the following equation, from [37]. The difference between the sending and receiving voltage (ΔV) is found from the above mentioned equation.

$$\Delta V = \frac{1}{V} \cdot (R_g \cdot P + X_g \cdot Q) \tag{8}$$

4.1 Plant design

In order to create a transfer function that is suitable for the control aspects found in Chapter 3 the methodology behind the principles is to be derived in this section. As found in previously sections a various number of parameters have an impact on the network. Therefore, these parameters such as grid voltage (V_g), short circuit ratio (SCR), and the XR ratio of the grid are to be investigated. This is to study the impact of the different parameters in the system and thereby estimate the total power losses.

Based on the estimated losses in the system it is possible to build a controller which can eliminate these losses. The power delivered in the PCC in the system can be defined

$$P_{out}^{PCC} = P_{out}^{HPP} - P_{loss}^{HPP} \tag{9}$$

Where P_{out}^{PCC} is the power output from the HPP at the point of common coupling, P_{out}^{HPP} is the power output from the hybrid power plant, that includes the production from the WF and PVP. The P_{loss}^{HPP} is the total amount of power losses in the system. The losses in the system can be expressed by the following function:

$$P_{loss}^{HPP}(V_g, P_{out}^{HPP}, Q_{out}^{HPP}, SCR, XR) \tag{10}$$

The hybrid power plant consists of multiple wind turbines and solar panels. Therefore, a simplification of the plant representation is need for control and tuning purposes. Moreover, wind turbines and solar panels are not expected to produce the same amount of power. This is due to the fluctuating wind speed and irradiation. These variations are expected to cause different loading and losses in the system. In order to overcome these challenges, the system must be simplified to a transfer function that is suitable for classical SISO theory. The production units and the load unit are designed similarly by a first-order transfer function and for the simplification, both WT and PV's are treated the same. The units are treated as a first-order transfer function with the time constants found the Chapter 3. It is expected that the dispatch of each unit (WPP and PVP) is distributing the power evenly between the generation units and the generation units are behaving equally. The diagram for of the units is shown in Figure 4.2.

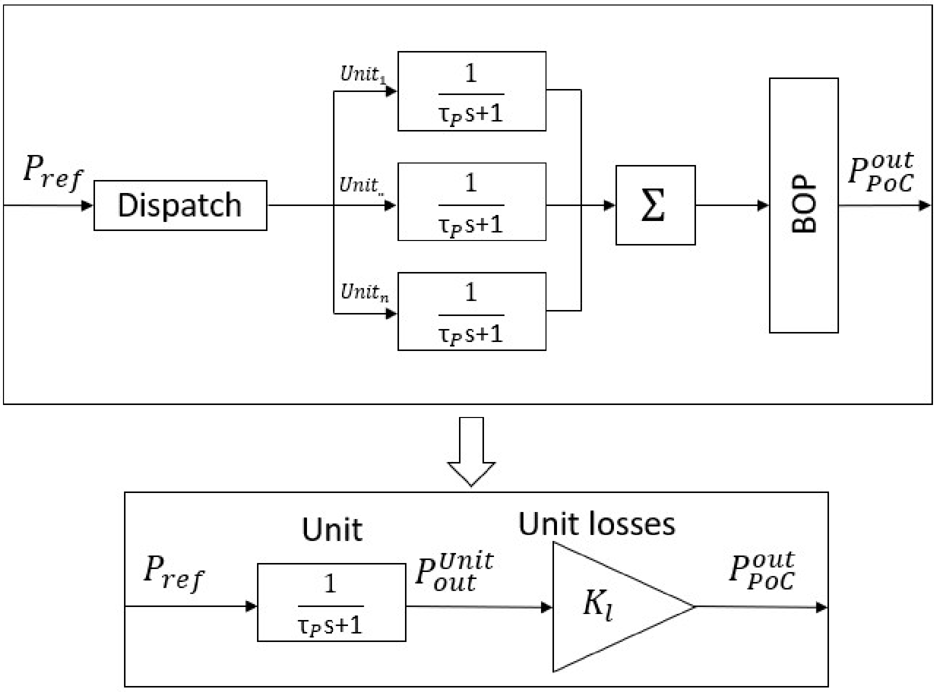

Figure 4.2: Active power transfer function for the units.

In order to develop a complete plant model for the HPP further simplification is needed. This is to apply classic SISO control theory for the whole plant. The WPP and PVP from Figure 4.2 are now presented as a first-order transfer function. Thereby the same approach can be done for the whole plant, as seen in Figure 4.3.

The hydrogen unit is treated as a first-order transfer function as seen from Chapter 3 and controlled by the dispatch. The unit does not contribute to the power production and based on the setpoints from the dispatch, excess power is consumed in the electrolyser. The balance of plant (BOP) represents the losses P_{loss}^{HPP} in the network, as found in equation 10.

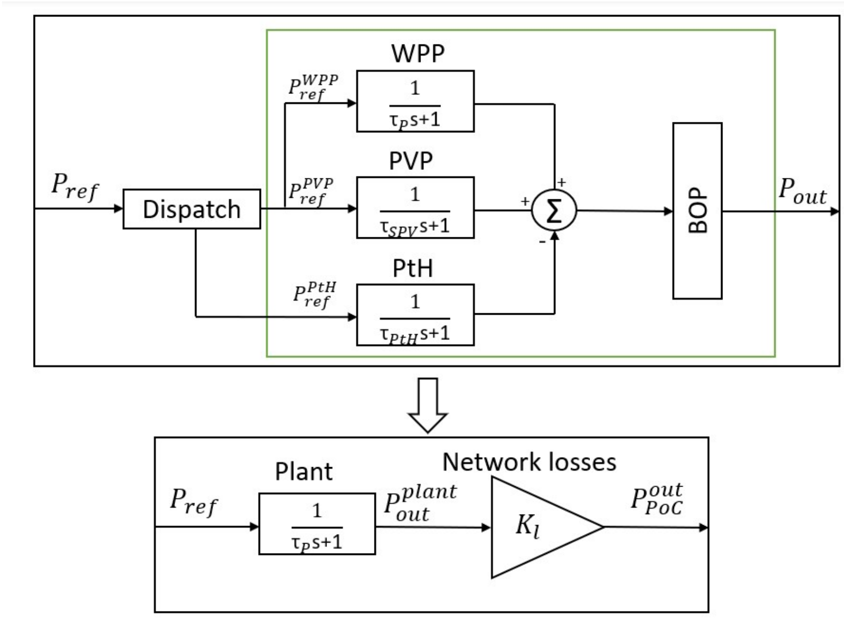

Figure 4.3: HPP active power transfer function.

In order to estimate the network losses for further control development, the following section is to investigate which parameters have the greatest impact on the losses in the network The load flow is based on WPP and PVP parameters described in Chapter 3. The external grid in the model is rated 60 KV and from technical regulation 3.2.5 and 3.2.2 the grid voltage (V_G) can very from 0.9 p.u to 1.10 p.u for both WPP and PVP [11] [12]. A typical value for SCR and XR ratio for a strong grid is considered to be 10 for both. These values is representing the external grid and may differ depending on sudden changes in the grid or inaccuracy. Therefore various test cases are obtained to map the losses under different scenarios in the grid. The test cases are addressed by the following parameters:

Test case 1: Power losses under normal operation conditions
Fixed values: SCR = 10, XR = 10, $Q_{HPP}^{out} = 0$
Ranging values: P_{HPP}^{out} varying 0.1 p.u for V_g [0.90 0.95 1 1.05 1.10] p.u

Test case 2: Power losses with varying SCR
Fixed values:, XR = 10, $Q_{HPP}^{out} = 0$
Ranging values: P_{HPP}^{out} varying 0.1 p.u for V_g [0.90 0.95 1 1.05 1.10] p.u and SCR between [5 10 15]

Test case 3: Power losses with varying XR
Fixed values:, SCR = 10, $Q_{HPP}^{out} = 0$
Ranging values: P_{HPP}^{out} varying 0.1 p.u for V_g [0.90 0.95 1 1.05 1.10] p.u and XR between [5 10 15]

Test case 4: Power losses with varying power to hydrogen plant
Fixed values:, SCR = 10, XR = 10, $P_{HPP}^{out} = 0.7$, $Q_{HPP}^{out} = 0$
Ranging values: P_{PtH}^{in} for V_g [0.90 0.95 1 1.05 1.10] p.u

4.1.1 Test case 1. Normal operation conditions

In this test case, the normal operation of the plant is to be obtained. The losses in the system are a function of the power output of the HPP, calculated at different external grid voltages. The SCR and XR ratio is kept at 10 and the losses for the system can be expressed as:

$$P_{HPP}^{loss} = (V_g, P_{HPP}^{out}) \tag{11}$$

In Figure 4.4 test case 1 is shown. The test case is to investigate the losses in the system under normal operations considered for this plant. The test is to show the external grids impact on the HPP. It is seen from the test that the highest losses are seen at $V_g = 0.9$ p.u when the lines are carrying the highest current and the lowest losses are seen when V_g is 1.1 p.u. At full load of the HPP ($P_{HPP}^{out} = 1$ p.u) the lines losses is increasing from 0.007 - 0.011 p.u for $V_g = 1.1$ p.u and $V_g = 0.9$ p.u, respectively. The test for normal operation indicates that the external grid has a significant impact on the losses in the system.

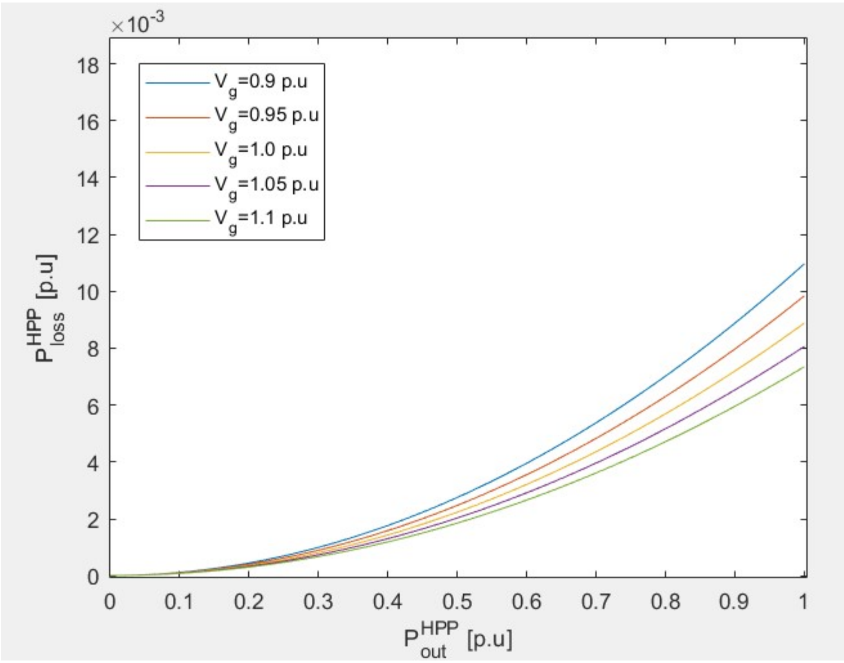

Figure 4.4: Test case 1: normal operation SCR=10, XR=10, P_{HPP}^{out} of 0.1 for V_g [0.9 0.95 1.0 1.05 1.1 p.u].

4.1.2 Test case 2. Power losses with varying SCR

In this test case, the impact of the SCR on the network losses is obtained, as seen in Figure 4.5. The power losses from the system are to be tested when the SCR is lowered to 5 and increased to 15. The SCR is one of the parameters defining the external grid from Equation 1 and is used for the impedance in Equation 3 and SCR is representing the stiffness of the grid. The test shows that the network losses are lower when the SCR=15 compared with SCR=5. The total losses for V_g in the network when P_{HPP}^{out} = 1 p.u for SCR=5 and SCR=15 is 0.015 and 0.007, respectively. This means that for a plant connected to a stiff grid the losses can be lowered.

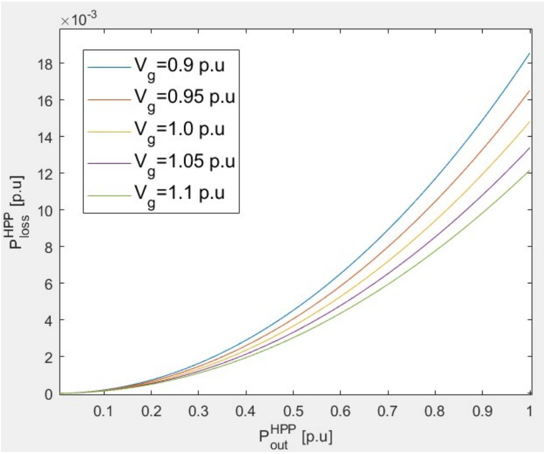

(a) Test case 2: network losses with SCR = 5

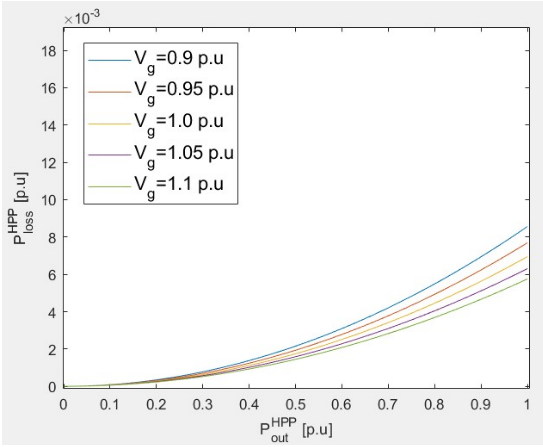

(b) Test case 2: network losses with SCR = 15

Figure 4.5: Test case 2: impact of different SCR [5 15]. XR=10, P^{out}_{HPP} increasing of 0.1 for V_g [0.9 0.95 1.0 1.05 1.1 p.u].

4.1.3 Test case 3. Power losses with varying XR

For test case 3 the impact of the XR ratio is to be tested. XR ratio is one of the parameters to define the external grid V_g and is tested for XR=5 and XR=15. From equation 3 XR ratio have a direct influence on the grid parameters and the test for XR=5 and XR=15 is seen in Figure 4.6. It is seen from the test, that by increasing the XR ratio, the losses in the system are decreased. From the two tests the losses under normal operation with $V_g = 1.0$ p.u and $P^{out}_{HPP} = 1.0$ p.u is 0.014 p.u for XR =5 and 0.007 p.u for XR = 15. The largest losses from the XR test are obtained when the external grid voltage is 0.9 p.u.

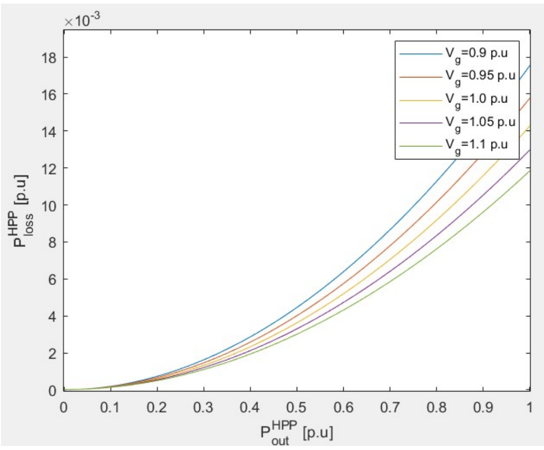

(a) Test case 3: network losses with XR = 5

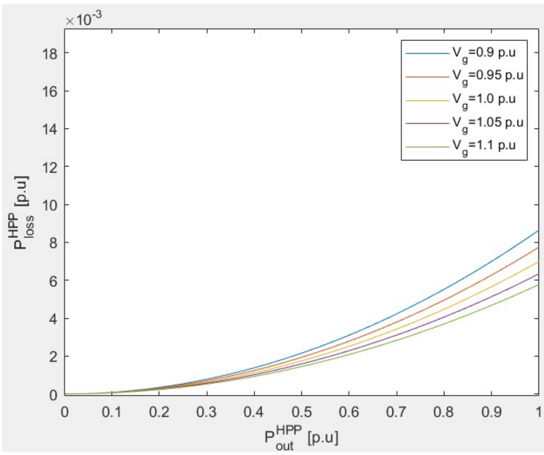

(b) Test case 3: network losses with XR = 15

Figure 4.6: Test case 3 impact of different XR [5 15]. SCR=10, P^{out}_{HPP} increasing of 0.1 for V_g [0.9 0.95 1.0 1.05 1.1 p.u].

4.1.4 Test case 4. Power losses with varying power to hydrogen production

In test case 4 the impact of the consumed power in the hydrogen plant is to be tested. The hydrogen plant is increased by 0.1 p.u and the losses in the system decreases, as seen in Figure 4.7. According to [34] the minimum load from the hydrogen is set to 0.05 p.u and at full load, the losses in the system are lowest. It is seen from the figure that the highest losses in the system is at $V_g = 0.9$, and the losses decreases from 0.0052 p.u to 0.0036 p.u. In the other hand, the losses are lowest when $V_g = 1.1$ and decreases from 0.0035 p.u to 0.0024 p.u.

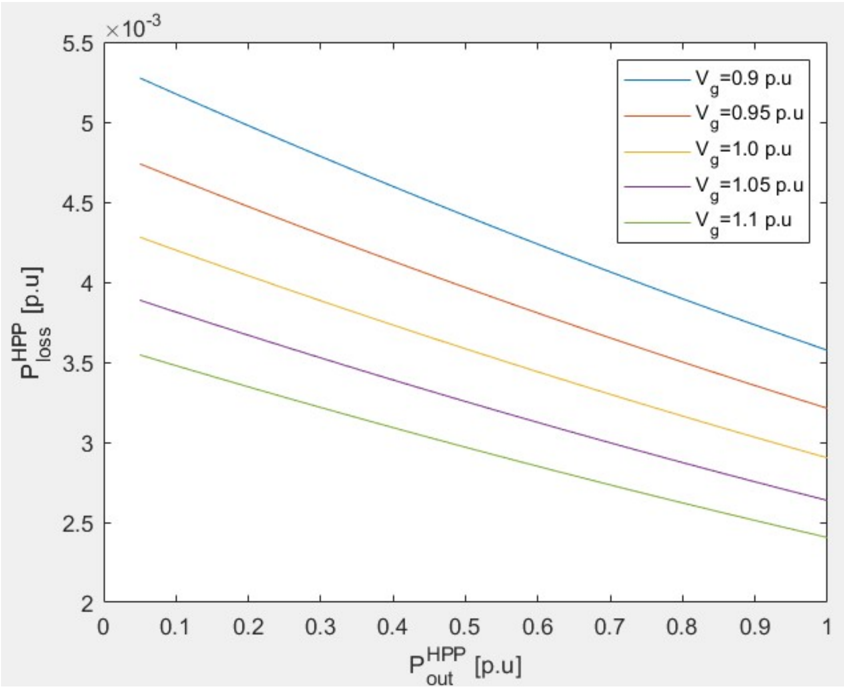

Figure 4.7: Test case 4: System impact of the PtH plant for V_g [0.9 0.95 1.0 1.05 1.1 p.u].

4.2 Summary

In this section, a simplified model of the HPP has been obtained. This is used for further analysis in order to design the plant controller for the system. Furthermore, the load flow studies of the system have been made. It is seen from the test that the external grid has a large impact on the losses in the network. Moreover, the parameters SCR and XR for the external grid have been obtained in order to study their direct impact on the system.
Lastly, the impact of the power consumption from the hydrogen plant has been obtained. The test showed that when the plant is operating at maximum power, the losses in the system are lowest. These results are used for further control design.

5 Chapter 5: Overview of grid codes and control system design

In this chapter, the grid codes for the wind power plant and PV plant are investigated for further system design. If any deviation between the two grid codes, worst-case scenario is chosen.

5.1 Danish grid codes for WPP and PVP

From technical regulation 3.2.2 [12] and 3.2.5 [11], the wind power plant and PV plant is separated into four categories. This is based on their nominal power and voltage magnitude. The four types of the plants are:

Table 5.1: Wind power plant and PV plant categories.

Category	WPP	PVP
A2	11 KW - 50 KW	11 KW - 50 KW
B	50 KW - 1.5 MW	50 KW - 1.5 MW
C	1.5 MW - 25 MW	1.5 MW - 25 MW
D	25 MW or <100 KV	25 MW or <100 KV

The wind power plant and PV plant presented in this network are rated 38 MW and 22 MW, respectively. This means that the requirements for the active power control design and frequency control design are based on the requirements for categories D and C.

Active power constraint functions

According to [11] all active power constraints must have an error less than 2 % for maximum 1 minute of the nominal power P_n in the PCC. This is considered as requirement for the HPP too.

Absolute power constraint is used to limit the active power at the PCC in order to avoid critical situations for overload on the grid. The setpoint for the plant is constant eventhough available power is higher than the setpoint. The activation should start within 2 seconds and be completed in less than 10 seconds.

Delta power constraint is also called spinning reserve and is used to limit the active power from the plant, based on the setpoint. This is used as a reserve in case of the frequency is dropping at PCC. The activation should start within 2 seconds and be completed in less than 10 seconds.

Ramp rate constraint is used to limit the maximum ramping rate for the plant. This is to avoid any fast disturbances due to the fluctuating production, which can cause undesirable stability situations. The limits for the ramp rate are set to 100 kW/s.

Control functions for active power

A wind power plant and PV plant must be installed with control functions to decrease the active power in PCC. This is done by a setpoint sent from the operating partners of the plant and grid. There are two types of control functions; frequency response and frequency control.

Frequency response is used to downscale the active power from the plant, based on the frequency at the PCC. This is activated whenever the frequency exceeds the grid frequency f_r. The f_r should have the possibility to be changed in the range of 50.00 HZ to 52.00 HZ. A common values for f_r is 50.20 Hz. The droop of the frequency response should be in the range of 2 % - 12 % of P_n. A common value for the droop is 4 %. Furthermore, the response should be initiated no later than 2 seconds and completed within 15 seconds after activation.

Frequency control function is used to control the frequencies above f_1 in order to stabilize the frequency at 50.00 Hz. Depending on the frequency control scaled, different values can be set for the droop in the intervals. The control function must initiate no later than 2 seconds and should be completed within 15 seconds. In case the P_n exceeds more than 10 % the response for the control may be down scaled. Furthermore, for frequency regulation above f_5 the plant can only decrease the active power until the frequency has decreased below f_7. The frequency control scheme is shown in Figure 5.1

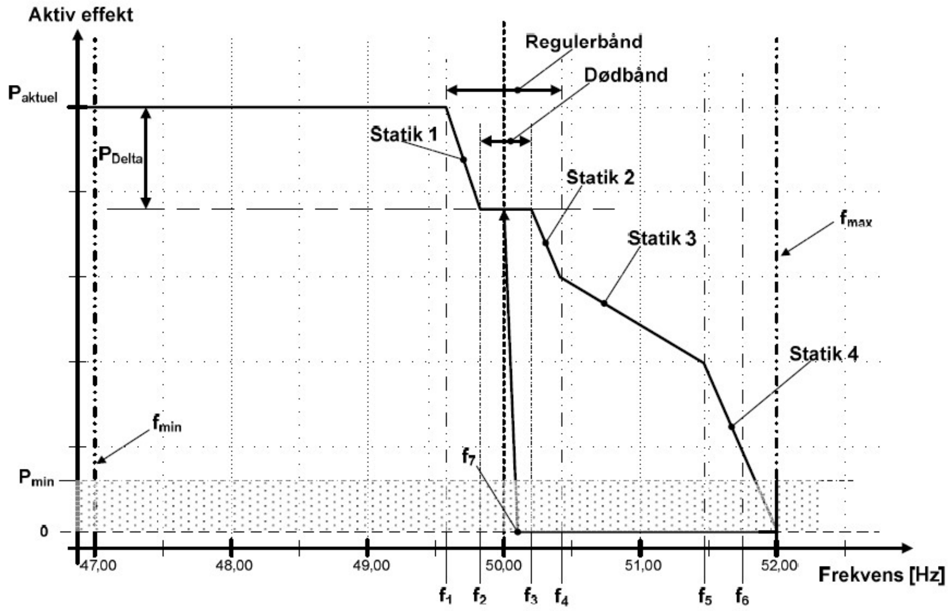

Figure 5.1: Frequency control function for WPP and PVP [12][11].

Based on the grid codes for WPP and PVP, respectively, a list of criteria is now set for the HPP based on the grid codes and is presented as follows:

- Settling time of < 10 s with steps of 0.1 p.u
- Steady state error of 2 % of P_n
- Maximum deviation of P_n of 2 % for 1 minute.
- The system must be stable

5.2 Control system design

From the criteria for the controller, a plant design is now shown in Figure 5.2. The plant design consists of the plant transfer function (including the losses in the system), a grid meter, and a controller. The error at PCC is measured by a grid meter and the error between the reference setpoint and the power at PCC is fed into the controller.

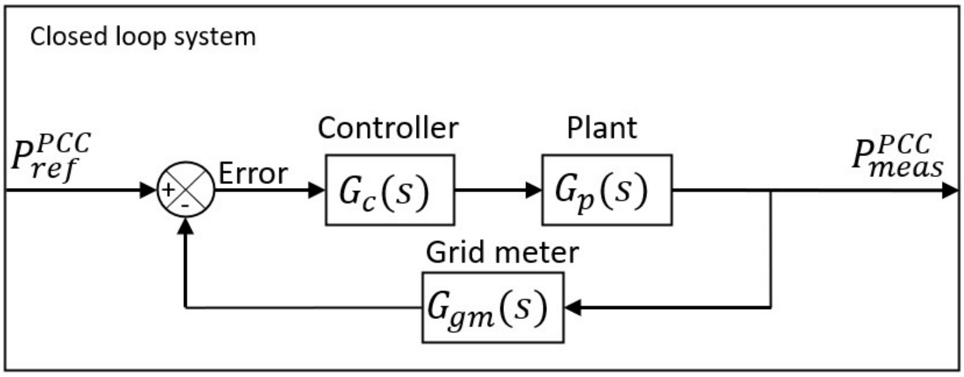

Figure 5.2: Closed loop system.

The closed loop transfer function of the system can be described as follows, based on [38].

$$G_{CL} = \frac{G_c(s)G_p(s)}{1 + G_c(s)G_p(s)G_{gm}(s)} \tag{12}$$

As obtained previously the plant transfer function can be described as:

$$G_p(s) = \frac{K_{loss}}{\tau_p s + 1} \tag{13}$$

The K_{loss} is the error between the input P_{ref} and the measured power at PCC P_{meas}^{PCC} and is described as:

$$K_{loss} = \frac{P_{out}^{HPP} - P_{loss}^{HPP}}{P_{out}^{HPP}} \tag{14}$$

As shown in the load flow analysis from Chapter 4, the losses in the system (K_{loss}) are varying, depending on the power output from the plant. In order to design the controller for the plant some assumptions must be taken into consideration. The parameters for the HPP under normal operation is assumed to be as following: $V_g = 1$ p.u, $P_{HPP}^{out} = 0.7$ p.u, SCR =10 and XR = 10. From Figure 5.3 the normal operation point is presented. At this point the total losses (K_loss) in the system is assumed to be $K_{loss} = 0.994$.

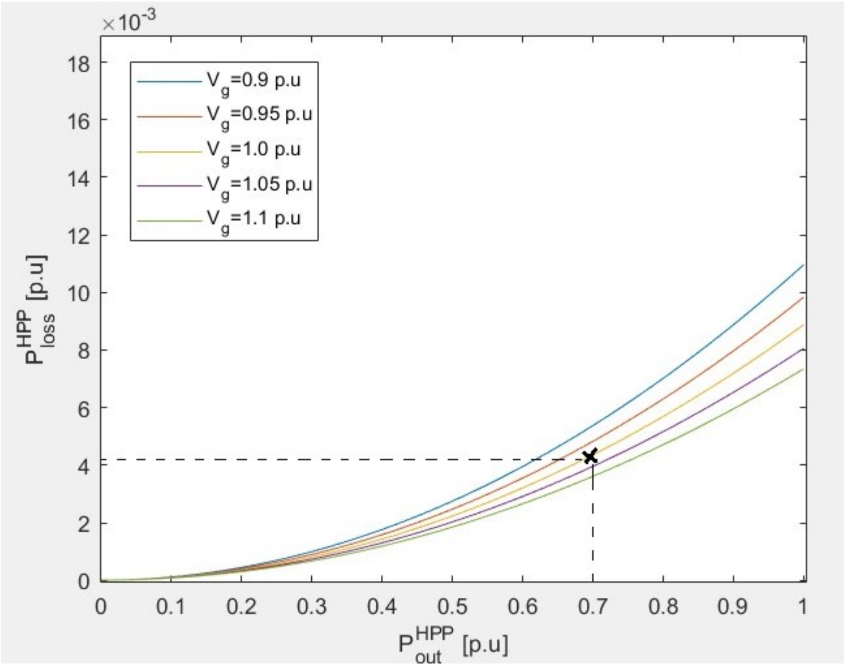

Figure 5.3: Operation point for controller design

The grid meter is represented by a lowpass filter and provides feedback signals to the controller from PCC. According to [39] and an appropriate value for the delay is 15 ms and the grid meter can be described as a first order transfer function. The grid meter is presented as:

$$G_{gm}(s) = \frac{1}{\tau_m s + 1} \tag{15}$$

The closed loop system for the hybrid power plant controller has now been presented with all parameters for further analysis. Different controllers are now to be investigated in order to find a control design that can obey the design criteria for the plant. The controllers that are to be investigated are presented:

- P - Controller
- PI - Controller

5.2.1 Proportional controller

In this section, a proportional controller is to be designed and verified. The performance of the controller is presented, and the results are discussed.

The transfers function of the proportional controller is:

$$G_c(s) = K_p \tag{16}$$

From equation 12 and 16 the closed loop transfer function of the system is presented.

$$G_{cl} = \frac{P^{PCC}_{meas}}{P^{PCC}_{ref}} = \frac{K_p K_{loss}(\tau_m s + 1)}{\tau_p \tau_m s^2 + (\tau_p + \tau_m)s + 1 + K_{loss} K_p} \tag{17}$$

From the closed loop transfer function the steady-state value is expressed as:

$$P_{meas}^{PCC} = \lim_{s \to 0} G_c l(s) P_{ref}^{PCC} = \frac{K_{loss} K_p}{1 + K_{loss} K_p} P_{ref}^{PCC} \tag{18}$$

Thereby an expression for the steady-state error for a step input is expressed as:

$$error = \frac{1}{1 + K_{loss} K_p} \tag{19}$$

The proportional gain for the system is presented in equation 20 as a result of P_{ref}^{PCC}. The K_p is found by choosing an appropriate value for the error that is allowed in the system.

$$K_p = \frac{\frac{1}{error} - 1}{K_{loss}} \tag{20}$$

From the design criteria found by the grid codes, the error in the system should be less than 2 % of P_n. In order to find an appropriate value for the proportional gain, the error is set to 1, 1.5, and 2 %.

In Figure 5.4 the root locus plot for the open loop system is shown. It is seen that the poles for the system are placed at -1 and -66.7, respectively. If the poles in the system are placed at the left half lane at the real axis in the root locus, the system is considered stable.

However, by increasing the gain of the system it is seen that the poles are changing to complex conjugated poles. This means that if the system is gained with more than 16.3 the system will cause an overshoot.

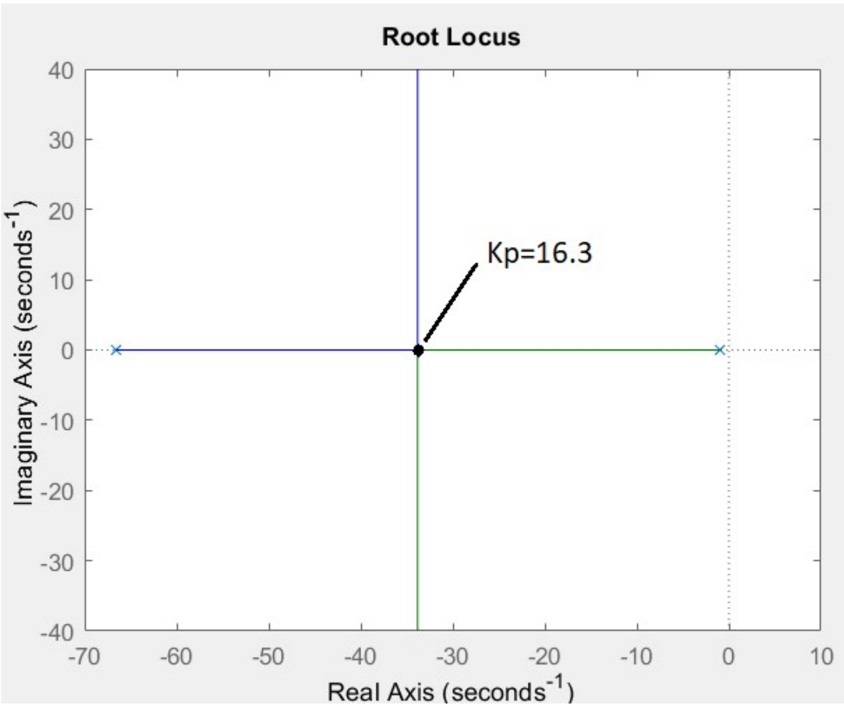

Figure 5.4: Open loop poles for $G_p(s)$.

As a design criterion, the system should not create an overshoot. For any K_p larger than 16.3 this will occur. In Table 5.2 the K_p for the maximum allowed error in the system is shown with the corresponding overshoot.

Table 5.2: Performance from the proportional controller.

Error %		Overshoot %
1	99.6	49
1.5	66.1	29
2	49.3	17.7

In Figure 5.5 a step response of 0.1 p.u of the system is shown. $K_p = 49.3$ which is the lowest value of K_p to satisfy the design criteria of a steady-state error of 2 %. However, from the step response, it is seen that an overshoot of 17.7 % is added to the system. From the control design, it is seen that the system should not include any overshoot. Therefore, even with the lowest values of K_p, the design criteria for the system are not fulfilled.

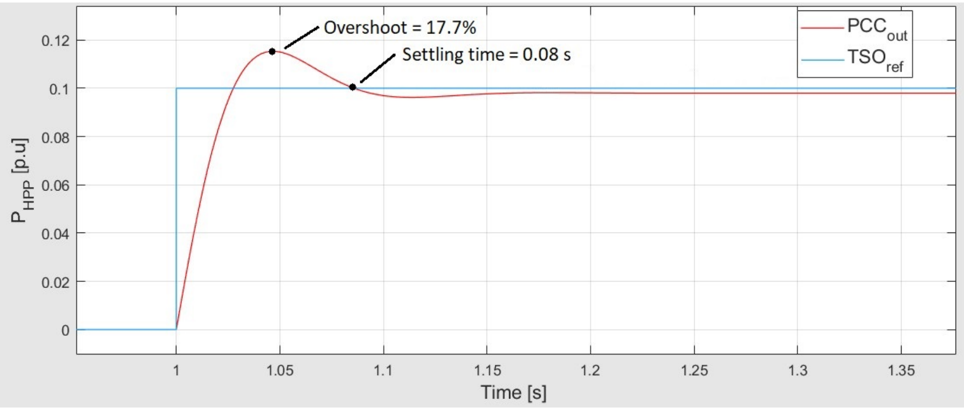

Figure 5.5: HPP step response of 0.1 p.u, Kp = 49.3.

It is seen from the step response that a proportional controller is not suited for the control design. By increasing the gain it is seen that the error is decreasing and the overshoot is increasing. By adding an overshoot to the system, the proportional gain is not suited as a controller.

5.2.2 PI- Proportional - Integral controller

The PI controller used for the system is based on the method *Modulus optimum* [6]. The principle of the method is to replace the slowest pole of the transfer function with a pole in the origin. In this case, the pole for the PI controller is placed at the same place as the plant transfer function. This means that the time constant for the PI is equal to the time constant for the plant. In equation 21 the PI transfers function is presented.

$$G_c(s) = K_p \frac{\tau_i s + 1}{\tau_i s} \tag{21}$$

As mentioned, the time constant for the PI controller is corresponding to the time constant for the plant transfer function

$$\tau_i = \tau_p \tag{22}$$

K_p is obtained as:

$$K_p = \frac{T_i}{K_{loss}} \tag{23}$$

The bode diagram of the controller, open loop, and closed loop system is shown in Figure 5.6. It is seen in the low frequency area of the closed loop system, that the pole from the grid meter does not have any impact. This is due to the phase shift from the pole being in the range of 1 decade before the bandwidth to 1 decade after the bandwidth. Furthermore, it is seen that the phase margin of the open loop system is > 90 degrees and the gain margin is above 3 dB. This indicates that the system is stable.

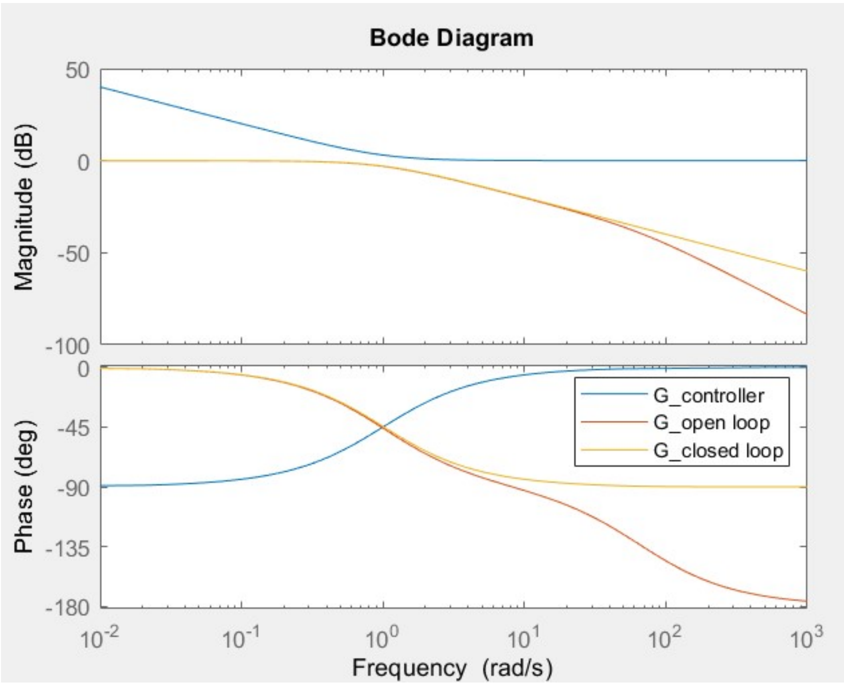

Figure 5.6: Bode plot of the controller, open loop and closed loop system.

The poles for the system are placed at -65.6, 1.02, and -1. Poles in the negative range of the real axis are an indication of a stable system. Furthermore, having the poles only at the real axis does also indicate that no overshoot is presented in the system.

In Figure 5.7 a step response of 0.1 p.u from the DSO is shown for the PI controller. It is seen in the figure that the controller does not have any overshoot and the settling time for the system is approximately 3.8 s and the steady-state error is 0.

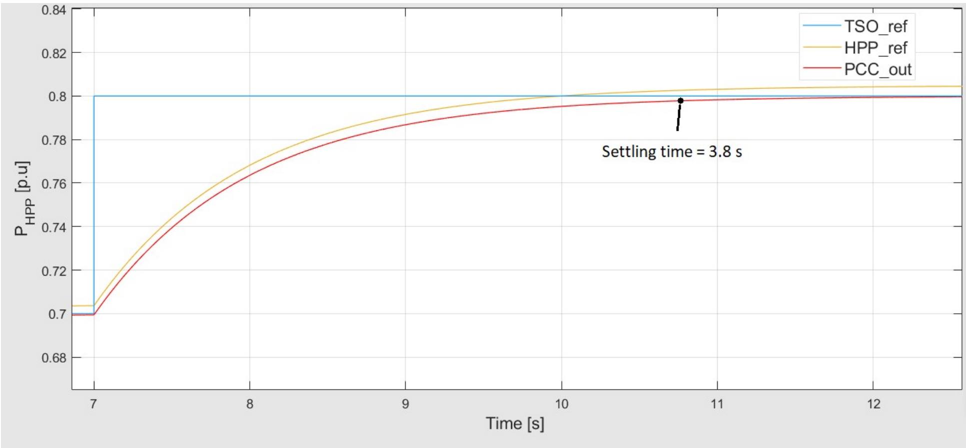

Figure 5.7: Step response of 0.1 p.u for the closed loop system with PI controller.

5.3 Proportional integral controller tuning

In Figure 5.8 the root locus for the open loop system is shown for the PI controller. It is seen that the system will have an overshoot when the gain exceeds 16.3. However, by increasing the gain for the controller, the bandwidth of the controller exceeds the bandwidth of the plant. In order not to exceed the plant bandwidth, the gain for the PI controller should be less than 1.

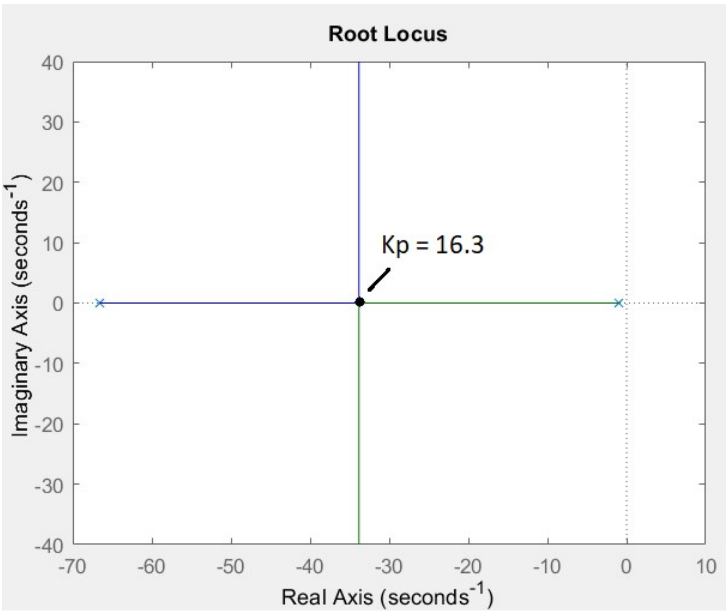

Figure 5.8: Root locus for the PI controller.

5.3.1 Pole-zero cancellation

The plant time constant for the HPP is chosen based on Chapter 3. It is seen that the plant time constant is assumed to be 1 s and the hydrogen plant time constant is assumed to be 2.5 s. Therefore, transient disturbances might occur when RPC is regulating the HPP according to the hydrogen plant. This means that a slower controller is affordable for the system.

By choosing a $\tau_i = \tau_p$ the system will follow the plant time constant. However, the system is operating a hydrogen plant at the same time, and the time constant for the hydrogen plant is slower than the production units. Assuming that the grid meters bandwidth does not have any larger impact on the system, the pole-zero cancellation is made with the controller ($G_c(s)$) and the plant ($G_p(s)$) transfer function. By choosing the zero in the numerator as the plant time constant τ_p, the controller is presented as:

$$G_c(s) = K_p \frac{\tau_p s + 1}{\tau_i s} \tag{24}$$

The transfer function for the PI controller and the plant is then:

$$G_c(s)G_p(s) = K_p \frac{\tau_p s + 1}{\tau_i s} \cdot \frac{K_{loss}}{\tau_p s + 1} = \frac{K_p K_{loss}}{s\tau_i} \tag{25}$$

The pole in the plant is then canceled by the similar chosen zero.

The pole in the denominator is then to be selected as a suitable value for the system. According to [38] the settling time for the plant is presented as:

$$bw = \frac{4}{\tau_i} \tag{26}$$

By choosing $\tau_i = 10$, the time constant for the controller is then 2.5 s, and will be within the grid codes.

The bode diagram of the tune controller is shown Figure 5.9. It is seen that the bandwidth is at 0.4 rad/s and the phase margin is still > 90 degrees. Furthermore, the gain margin is above 3 dB. These factors indicate that the system is stable.

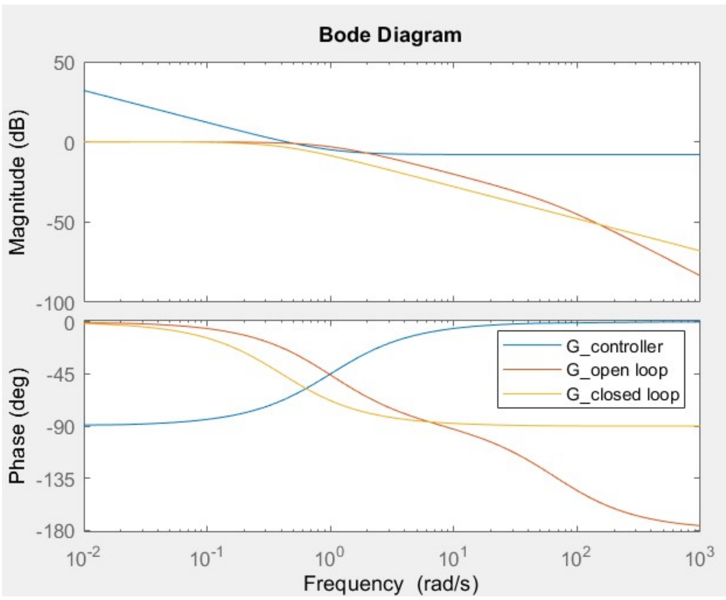

Figure 5.9: Bode diagram of tuned PI controller.

The poles for the tuned controller are now placed at -66.3, -1, and -0.4. With poles in the negative range of the real axis, is also an indicates that the system is stable.

In Figure 5.10 a step response of the tuned PI controller is shown. It is seen that the settling time for the controller i 9.7 s. This is 5.9 s slower than the original PI controller without pole-zero cancellation. The controller is still within the limits of the grid codes and does not add any overshoot to the system.

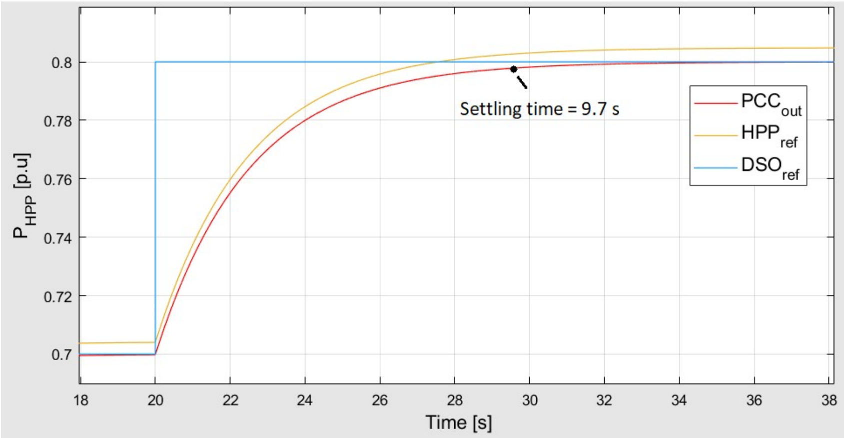

Figure 5.10: Step response of the tuned PI controller with step of 0.1 p.u.

5.4 Test and verification of the active power controller

The active power controller is designed assuming that the system operates under normal conditions with a stable grid. A stable grid in this case is considered as a $V_g = 1$ p.u, SCR = 10 and XR = 10. However, extreme scenarios might occur under operation. Therefore, the robustness of the controller is to be tested to verify whether the controller is compatible with the scenarios. Two test scenarios are to be investigated. The first scenario is to test the controller under different grid voltage and grid parameters. Thereby, the robustness of the controller can be verified. The second scenario is to test the different operation modes the HPP can operate, where the production from the WF and PVP is distributed equally. These operation modes are defined from the grid codes and used for the overall operation of the plant.

- Test scenario 1
  - Test case 1: Varying power production
  - Test case 2: Varying grid voltage
  - Test case 3: Varying SCR
  - Test case 4: Varying XR
- Test scenario 2
  - Test case 1: Absolute power constraint
  - Test case 2: Delta power and ramp rate constraint
  - Test case 3: Frequency response
  - Test case 4: Frequency control

5.4.1 Test scenario 1

In this test case, the controller is tested for different reference setpoints. This is to verify the robustness of the controller. It is seen in Figure 5.11a and 5.11b that the power reference is changed from 0.2-0.3 and 0.8-0.9 p.u, respectively. The parameters for the network is considered as normal, which in this case means: $V_g = 1$ p.u, SCR = 10 and XR = 10. For both tests is it seen that the controller can eliminate the error and is sending out the requested amount of active power at PCC. The settling time is approximately 9.7 s. It is seen that the settling time from the test fulfills the specifications from the grid codes and system does not have any overshoot.

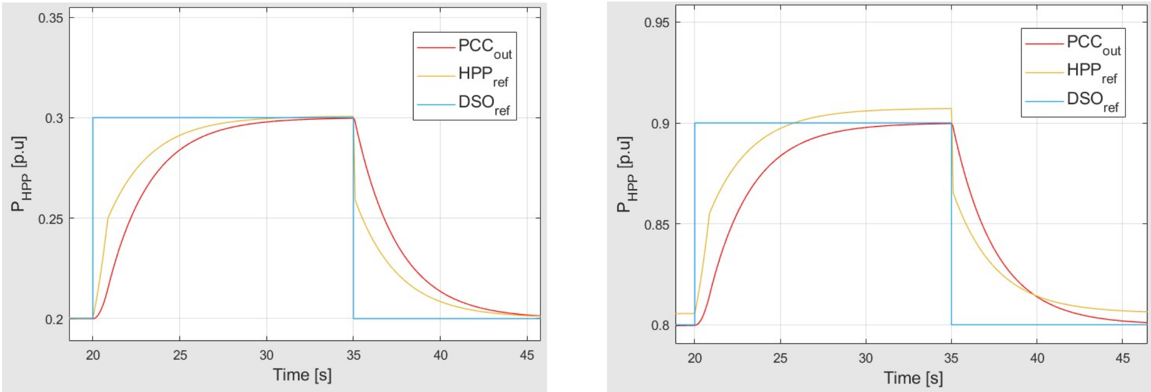

(a) Test case 1 step of 0.1 p.u. From 0.2-0.3 p.u

(b) Test case 1 step of 0.1 p.u. From 0.8-0.9 p.u

Figure 5.11: Test case 1 with different step input.

In this test case, the performance of the controller is tested with different grid voltage. This is to ensure that the controller can eliminate the error in the network at the minimum and maximum allowed voltage caused by the external grid. Therefore the test of voltage level V_g = 0.9 and 1.1 p.u is tested. The parameters for the network are SCR = 10 and XR = 10. In Figure 5.12a and 5.12b it is seen, that the controller is eliminating the error and keeps the PCC_{out} at the requested setpoint. This is for both V_g = 0.9 and 1.1 p.u. Furthermore, it is seen that the settling time is approximately 9.7 s and there is no overshoot in the system. The controller design is robust enough to withstand scenarios of different grid voltage.

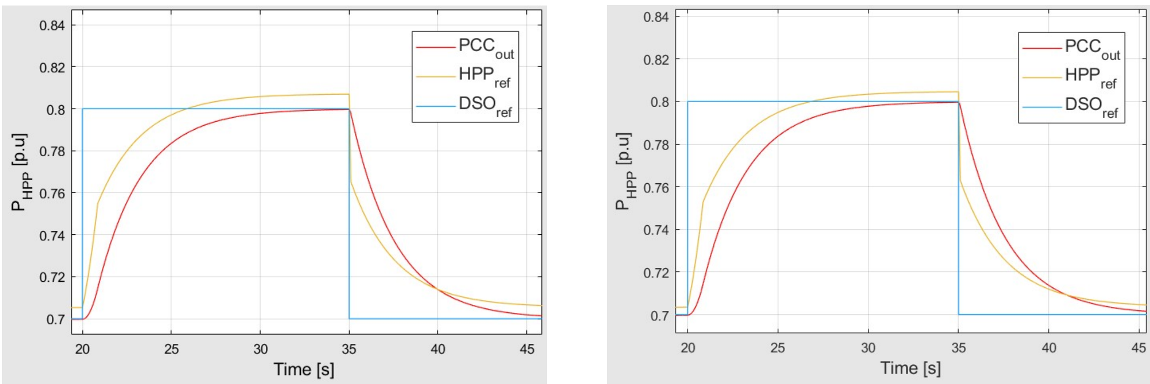

(a) Test case 2 step of 0.1 p.u. V_g = 0.9 p.u

(b) Test case 2 step of 0.1 p.u. V_g = 1.1 p.u

Figure 5.12: Test case 2 with different grid voltage.

In this test case, the controller is tested for different SCR parameters. The design of the controller is based on an SCR = 10. Therefore, in case of disturbances or inaccuracy of the SCR, different values are tested. The selected values for the test is SCR = 5 and 15. The settings for the network are V_g = 1.0 p.u and XR = 10. The response of the controller is shown in Figure 5.13a and 5.13a, for SCR = 5 and 15. It was found in Chapter 3 that an SCR = 5 will cause the highest losses in the system. It is seen that the controller can eliminate the error for both SCR = 5 and 15, respectively. Furthermore, the settling time is approximately 9.7 s and does not exhibit overshoot. This means that the controller is robust enough to withstand disturbances for a certain range of inaccuracy of the SCR.

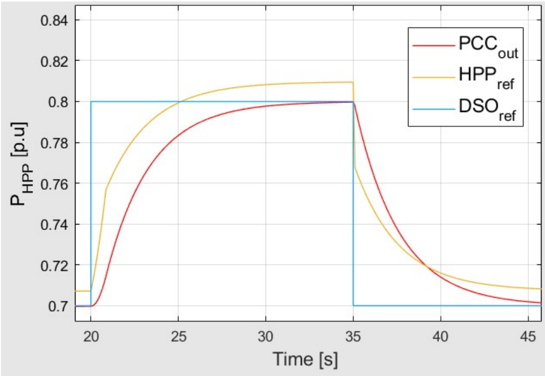

(a) Test case 3 step of 0.1 p.u. SCR = 5

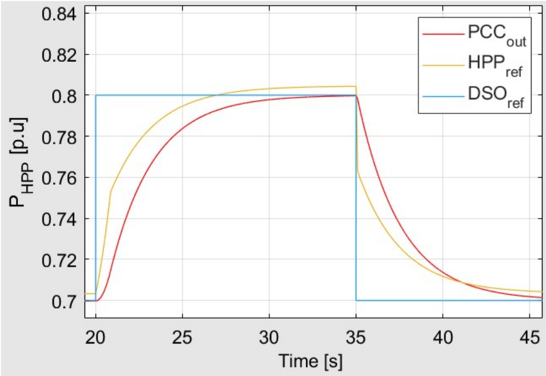

(b) Test case 3 step of 0.1 p.u. SCR = 15

Figure 5.13: Test case 3 with different SCR.

In this test case, the impact of different XR ratios is to be tested. The controller is tested for both XR = 5 and 15 and the parameters for the network are $V_g = 1.0$ and SCR 10. It is seen in Figure 5.14a and 5.14b that the controller is eliminating the error for both XR = 5 and 15. Furthermore, the settling time is approximately 9.7s and there is no overshoot in the system.

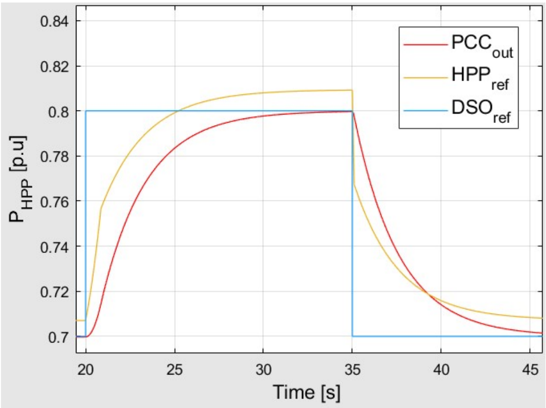

(a) Test case 4 step of 0.1 p.u. XR = 5

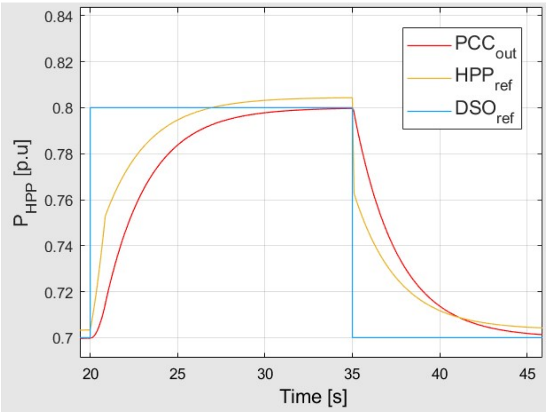

(b) Test case 4 step of 0.1 p.u. XR = 15

Figure 5.14: Test case 4 with different XR ratio.

5.4.2 Test scenario 2

In this test scenario, the active power constraints and frequency control functions are to be tested. For all test cases, the available power is kept constant. The reference setpoint from the operator or DSO is varying in order to test the dynamic of the controller. The HPP is based on active power production from both wind turbines and PVs. The dispatch is distributing the setpoint to the production units based on the available power in the plant. When the plant is operating and excess available power occurs, the power is sent to the electrolyser to maximize the utilization of the available power. The main goal of the test is to show the plant is able to operate according to the grid codes and utilize excess power in the system. The active power sent to the PCC should therefore be equal to the setpoint sent from the operator within the limited time frame and criteria. Furthermore utilizing excess power in the electrolyser should not cause any disturbances in the PCC.

Test of absolute power constraint with step of 0.1 p.u
In Figure 5.15 the absolute power constraint is tested. The power from the WF and PVP is producing 1 p.u for the test, respectively. The HPP is producing absolute power of 0.7 p.u based on the reference setpoint from the DSO. At 50 seconds, a step down from the DSO of 0.1 is shown. When the step down occurs, it is seen that the HPP follows the new setpoint from the DSO at the PCC and HPP is distributing the excess available power to the PtH (electrolyser). The settling time is less than 10 seconds and no overshoot is introduced to the system. According to the plant design, this is within the allowable range for the controller. At 70 seconds the setpoint from the DSO is changed with a step-up of 0.1 p.u. The HPP is following the new setpoint with a settling time of less than 10 s without exhibit overshoot. In this test, the HPP plant is producing more power than needed in PCC. This is due to the excess available power in the system is consumed by the PtH plant. When the step changes occur it is seen that the HPP is curtailing the power but manages to keep full utilization of the PtH plant without any disturbances at PCC.

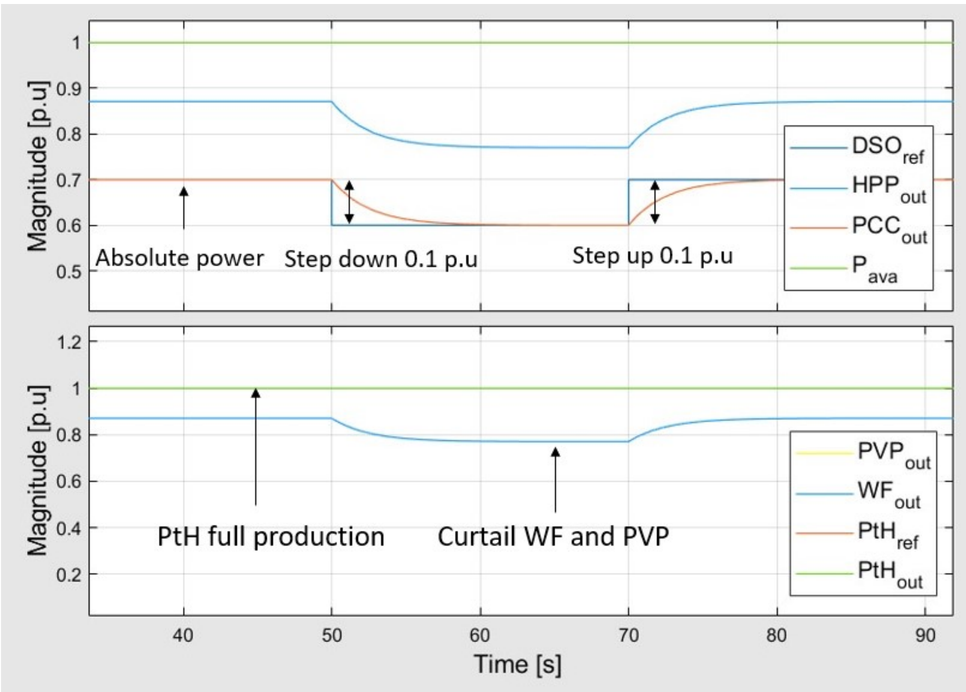

Figure 5.15: Absolute power constraint with step of 0.1 p.u

Test of delta constraint (spinning reserve) including ramping of 100 kW/s

In Figure 5.16 the test of delta power constraint and ramping constraint is shown. At 50 seconds the setpoint sent from DSO is ramping down to follow the new setpoint. According to the grid code, this should be 100 kW/s corresponding to 0.00167 p.u/s for the plant. At 200 seconds the new setpoint is reached with a delta from the reference setpoint. The power output from the plant increases again at 300 seconds with a ramping up of 0.00167 p.u to follow the setpoint sent from the DSO. From the figure, it is seen that the power output from the HPP is higher than the power output at PCC. This is due to the electrolyser consuming the excess available power in the system. When the power output at PCC is curtailing, it is seen that the power output from the HPP is decreasing too and utilizes the excess available power for the electrolyser. At 450 seconds the PCC output is following the setpoint from the DSO once again without disturbances from the electrolyser.

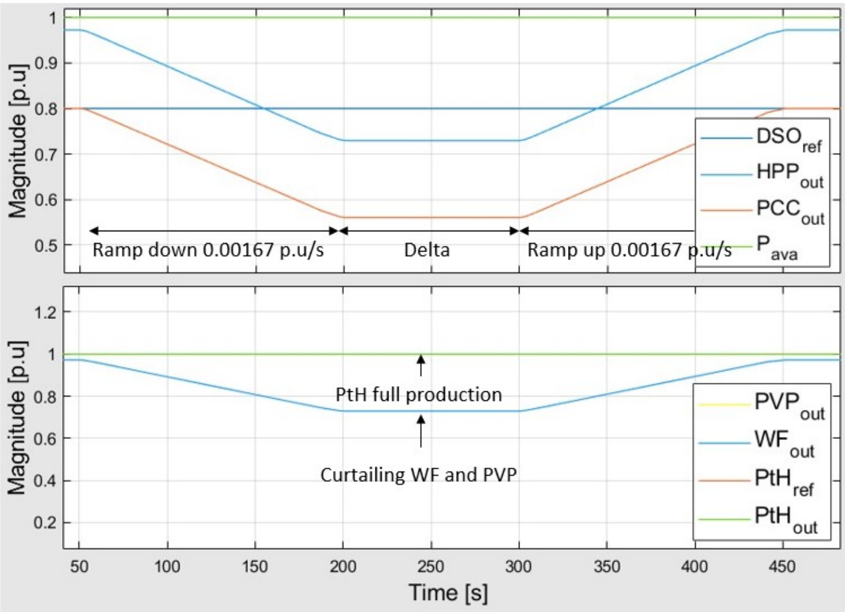

Figure 5.16: Delta power constraint

Test of frequency response

In Figure 5.17 the frequency response function is shown. The purpose of the test is to curtail the power production when the frequency exceeds F_R. At 70 seconds, it is seen that the power output at the PCC curtails when $F_R = 50.2$ Hz. The power output from the HPP remains at full production and ramping up the electrolyser. This means that the HPP is utilizing the excess available power, while the power output at PCC fulfills the grid codes. At 140 seconds the power output at PCC = 0, and excess available power is utilized in the PtH. At 150 seconds the frequency starts to decrease and the power output at PCC increases. This means, that more power is needed at PCC and the active power consumed in the PtH is curtailed to meet the setpoint.

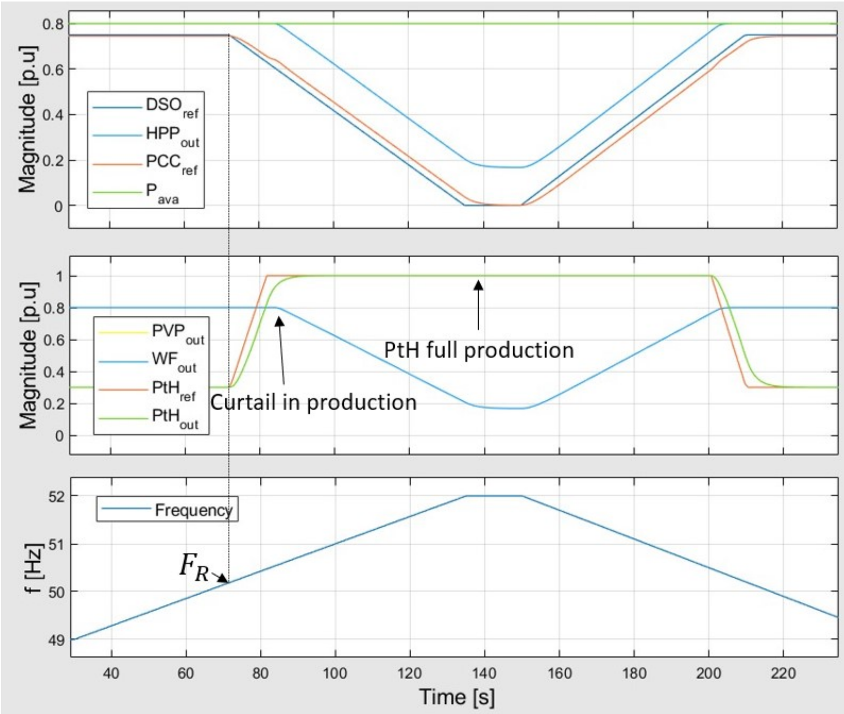

Figure 5.17: Frequency response with electrolyser.

Test of frequency control
In Figure 5.18 the test of the frequency control is shown. Likewise, the frequency response, the purpose of the frequency control is to curtail the power production at PCC when the frequency increases. The main difference between the response and the control is that the HPP should curtail with different droops at different frequencies. The frequency control should also include a dead band around 50 Hz. When the frequency reaches $f_6 = 52$ Hz the power output at PCC remains 0 until the frequency drops below $f_7 = 50.1$ Hz again. When the frequency drops below f_7, the power output at PCC increases again to meet the reference setpoint from the DSO.
From the test, it is seen that the power output at PCC is curtailing while the frequency increases. While the power output at PCC decreases, the excess available power is distributed to the PtH and when the power consumption from PtH = 1 p.u, the power output from the HPP starts to decrease. When the frequency drops below $f_7 = 50.1$ Hz the power output at PCC increases again and the power consumption in the PtH decreases. It is seen in the figure, that the power output at PCC is not affected by the power consumption from the PtH plant. In case of the frequency increases, the HPP is able to utilize the available power in the plant, while the grid codes at PCC have been complied with.

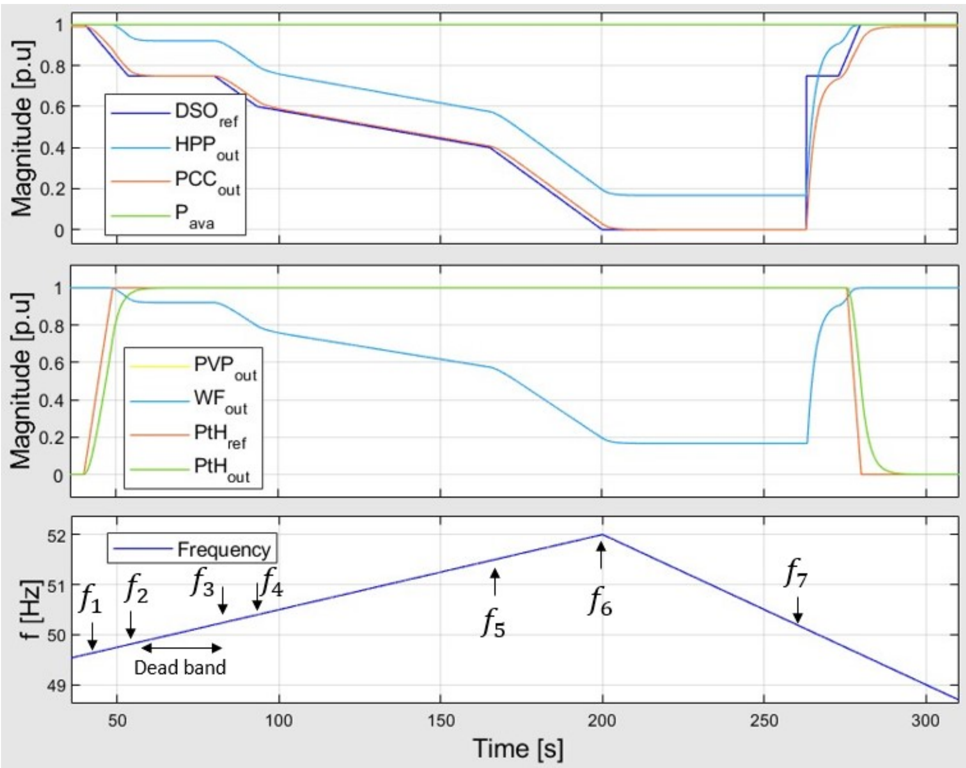

Figure 5.18: Frequency control

5.5 Different dispatch strategies

Due to the different production profiles of the production units, different dispatch strategies are investigated. The first method, proportional dispatch, is based on the available power from each plant. Thereby the production is adjusted based on the weather and the time of the day. However, in some cases, it can be affordable to let the wind turbines produce full power, while the power production from the PVs is curtailed. Due to the power electronics from the PVs, the time response is much faster than the wind turbines. By letting the WTs produce maximum power, the PVs can be used to adjust for disturbances in the system instead.

In Figure 5.19 test case 2 with ramping up/down and delta constraint is shown with proportional dispatch. The PVP is producing 0.7 p.u and the WF is producing 0.6 of rated production. The power production from the WF and PVP is now based on the available power from each unit. This means that the power output from the HPP is adjusted by both the WF and the PVP. This could lead to extra stress on the mechanical parts inside the WTs. Therefore, a strategy of letting the wind produce maximum and then adjust the power output from the HPP by the PVs could be affordable.

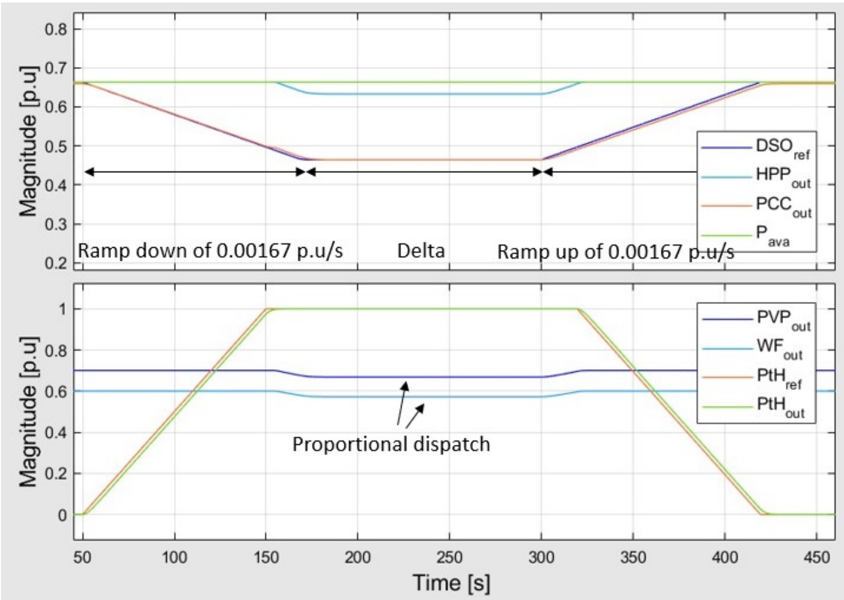

Figure 5.19: Delta power constraint with proportional dispatch

In Figure 5.20 the test case of ramping up/down with delta power constraint is shown. In this figure, the power output at PCC is adjusted by the PVs, while the WF is producing maximum available power of 0.7 p.u. This is to lower the stress on the mechanical parts inside the wind turbine and let the PVs control the power output. The power output at PCC is still following the setpoint from the DSO but in this test, only the PV is decreased to follow the setpoint at PCC. By using this method not only the mechanical stress on the wind turbine is lowered. The time response from the power electronic inside the PV is reacting faster than the mechanical parts in the WT and could be used to adjust the power in case of disturbances.

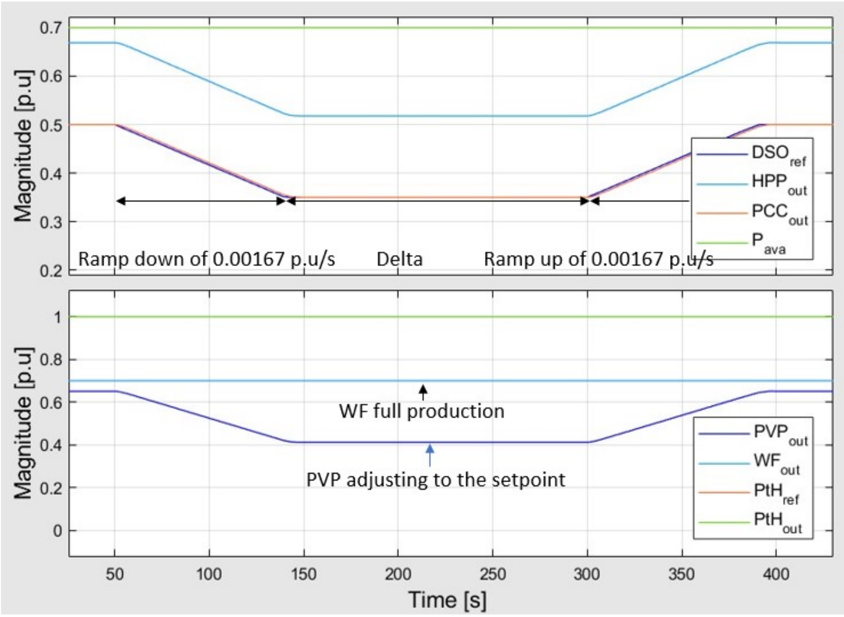

Figure 5.20: Delta power constraint with maximum utilization of the wind power.

5.6 Summary

In this chapter, plant design criteria have been designed according to the danish grid codes for active power and frequency control. From network studies, it was found that power losses in the system were introduced at PCC when operating the HPP. The maximum allowed power loss at PCC is 2 % which means that a controller is needed to eliminate this error. Two controllers have been investigated in order to cancel the error in the system. A proportional and a proportional-integral controller were investigated in the continuous time domain. It was seen that the P controller had a large overshoot in the system in order to fulfill the 2 % criterion. Therefore a PI controller has been designed in order to eliminate the error without overshoot. The PI controller design was based on Modulus Optimum method. From the plant design, it was seen that the electrolyser had a time constant slower than the production units WT and PV. Therefore the PI controller has been designed in order to match the time constant from the electrolyser plant of 2.5 s. The robustness of the controller has then been tested in order to ensure that the controller is able to eliminate the error in worst-case scenarios, where the losses in the system are highest. In order to verify the controller and the performance under operation scenarios, several test cases have been made. The results of the tests shows that the HPP is able to follow absolute power constraint and follow the reference setpoint for a ramp up/down of 0.1 p.u. The test shows that the power output from the HPP is higher than the power output at PCC. This is due to the PtH that was consuming the excess available power in the system. The results from the ramping up/down test with delta constraint showed that the controller is able to ramp up and down according to the grid codes of 100 kW/s. It was seen from the test that the power output at the HPP was higher than the power output at PCC due to the power consumption of the electrolyser. Furthermore results from the frequency response and control shows that the output at PCC is curtailing while the frequency increases. Moreover, it was seen that the PtH plant was utilizing the excess available power in the system and curtailing when the demand at PCC was needed. Lastly, two different dispatch strategies have been tested to regulate the power output at PCC. It is seen that with proportional dispatch both the WTs and the PVs were controlled in order to meet the requirements at PCC. For the second strategy, the power output from the WTs is kept at maximum production, and the regulation at PCC is done by the PVP. This strategy should lower the stresses on the mechanical part of the wind turbine and utilize the fast response from the PV.

6 Chapter 6: Implementation of discrete controller

To implement a controller to an HPP, the controller is transformed into a discrete controller. The discrete controller consists of a discrete transfer function with a sampling time. Therefore, the closed loop system of the discrete controller is investigated, in order to verify the performance. According to [24] the sampling time of the controller is depended on the details from the HPP. For a simple HPP model, a sample time of approximately 10 s is recommended and for a more detailed model, a sampling time of approximately 1 s is recommended. A sampling time of 10 s is too high for the proposed model and a sampling time of 1 s is chosen for the controller. In Figure 6.1 a block diagram of the discrete system is seen.

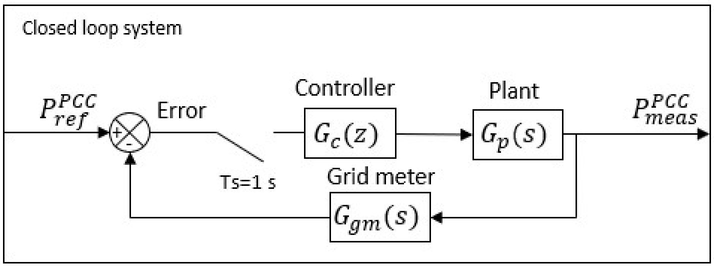

Figure 6.1: Block diagram with discrete controller.

6.1 Discretization methods

When going from the continuous domain to the discrete domain different approaches can be utilized. In Figure 6.2 three discretization methods are shown. To transform from the continuous domain to the discrete domain the s-term is replaced by the z-term in the table, where T_s is the sample time. According to [40] utilizing the Forward Euler method in some cases might cause instability. Therefore, the test is carried out by the Backward Euler and Tustin methods.

Backward Euler	Forward Euler	Tustin
$s = \frac{z-1}{T_s z}$	$s = \frac{z-1}{T_s}$	$s = \frac{2}{T_s}\frac{z-1}{z+1}$

Figure 6.2: Discretization methods [40].

To implement the discrete PI controller in the system, the controller is presented in canonical form.

$$G_c(z) = \frac{b_0 + b_1 z^{-}1}{1 - a_1 z^{-}1} \tag{27}$$

The parameters a_0, b_0 and b_1 for the PI controller without pole-zero cancellation is found in Figure 6.3.

	a_1	b_o	b_1
Backward Euler	1	$\frac{KpT_s}{T_i} + Kp$	$-Kp$
Forward Euler	1	Kp	$\frac{KpT_s}{T_i} - Kp$
Tustin	1	$\text{Kp}\left(\frac{T_s}{2T_i} + 1\right)$	$\text{Kp}\left(\frac{T_s}{2T_i} - 1\right)$

Figure 6.3: Parameters for the canonical form without pole-zero cancellation.

From the pole-zero cancellation, the new parameters for the discrete PI controller are found. The time constant T_c is now included in the parameters b_0 and b_1. These are shown in Figure 6.4.

	a_1	b_o	b_1
Backward Euler	1	$\frac{KpT_s}{T_c} + \frac{KpT_i}{T_c}$	$\frac{KpT_i}{T_c}$
Forward Euler	1	$\frac{KpT_i}{T_c}$	$\frac{KpT_s}{T_c} - \frac{KpT_i}{T_c}$
Tustin	1	$\text{Kp}\left(\frac{T_s}{2T_c} + \frac{T_i}{T_c}\right)$	$\text{Kp}\left(\frac{T_s}{2T_c} - \frac{T_i}{T_c}\right)$

Figure 6.4: Parameters for the canonical form with pole-zero cancellation.

From equation 27 a block diagram of the PI controller is represented. This is used to implement the controller into the HPP model and is shown in Figure 6.5.

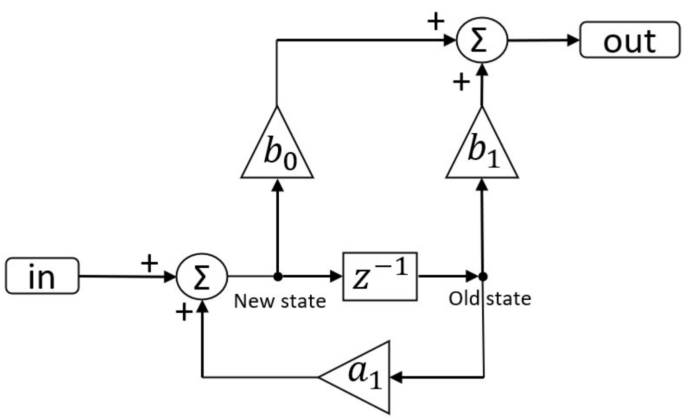

Figure 6.5: Block diagram of canonical expression.

The new state in the block diagram is based on the new input of the system and the previously state (old state). In the first sample the previously state is = 0. The calculation of the new state is shown in the following equation:

$$newstate = in + oldstate \cdot a_1 \tag{28}$$

The output of the controller is then based on the newstate and the oldstate. This is shown in the following equation:

$$out = newstate \cdot b_0 + oldstate \cdot b_1 \tag{29}$$

One of the advantages of using the canonical form is the simplicity of changing the parameters for the controller. This can be done by changing the parameters. Thereby, no further z transformation is needed.

The purpose of the controller is to create the same out for the HPP as a continuous PI controller. This is to avoid any overshoot at the PCC and to make the fast responding WTs and PVs equal to the slower responding electrolyser. In Figure 6.6 the discrete PI controller based on the Backward Euler and Tustin method is shown with a sample time of 1 s. The settling time for the Backward Euler has been increased to approximately 10.7 s. This means that the system has become slower and does not fulfill the design requirements. Therefore some fine-tuning is needed for the method to generate an output for the HPP with a settling time of approximately 10 s. For the Tustin method, it is seen that the system has become faster. This means that the settling time has decreased to approximately 8 s and fine-tuning is needed for the Tustin method too.

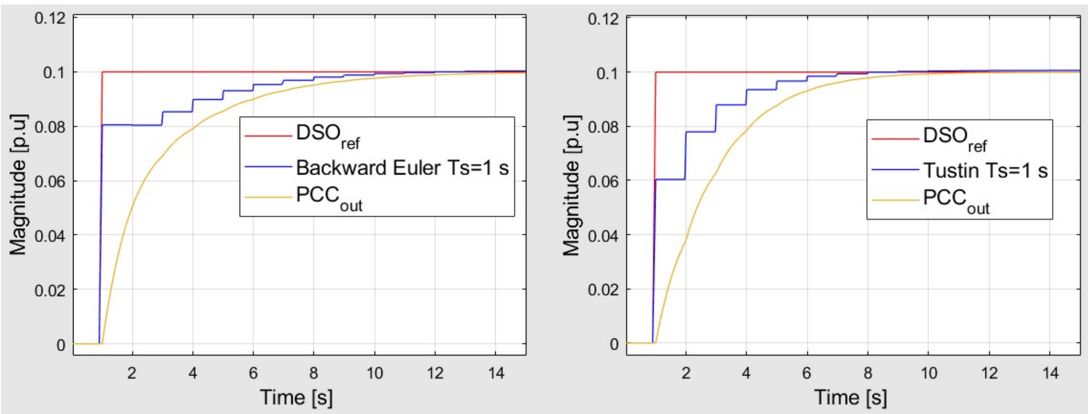

Figure 6.6: Step response for Backward Eueler and Tustin method.

For the Backward Euler method, a faster settling time is needed to fulfill the controller requirements. For the Tustin method, a slower settling is needed. Kp in the continuous domain is the same as Kp in the discrete domain. In order to fine-tune the controller for each methods, Kp can be adjusted to increase or decrease the bandwidth for the controller. Due to the canonical expression for the discrete controller Kp is simply changed in the parameters for b_0 and b_1. This is seen in Figure 6.7 where the fine-tuning of the controller is shown. For the Backward Euler method, Kp is increased to 1.1, and the new settling time is approximately 9.7 s. For the Tustin method, Kp is adjusted to 0.86, and a new settling time for the HPP is approximately 9.7 s.

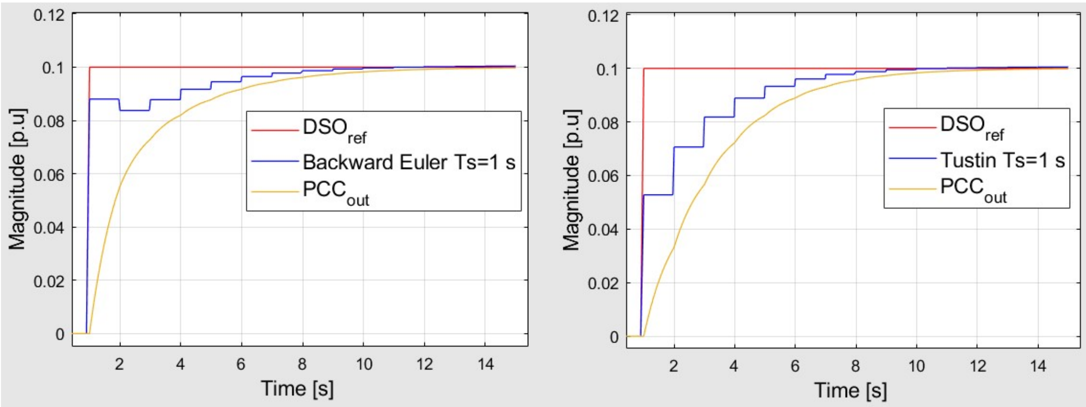

Figure 6.7: Fine tuning of the discrete controller.

A comparison of the two fine-tuned methods has been made to investigate the controller capability of matching the PtH plant. This is seen the Figure 6.8, that both the Backward Euler and Tustin method is able to meet the settling time of approximately 10 s with a sample time of $T_S = 1$ s. However, the Tustin method is almost identical to the PtH transfer function compared to the Backward Euler method. To avoid unwanted disturbances the design of the discrete controller for the HPP is made by the Tustin method.

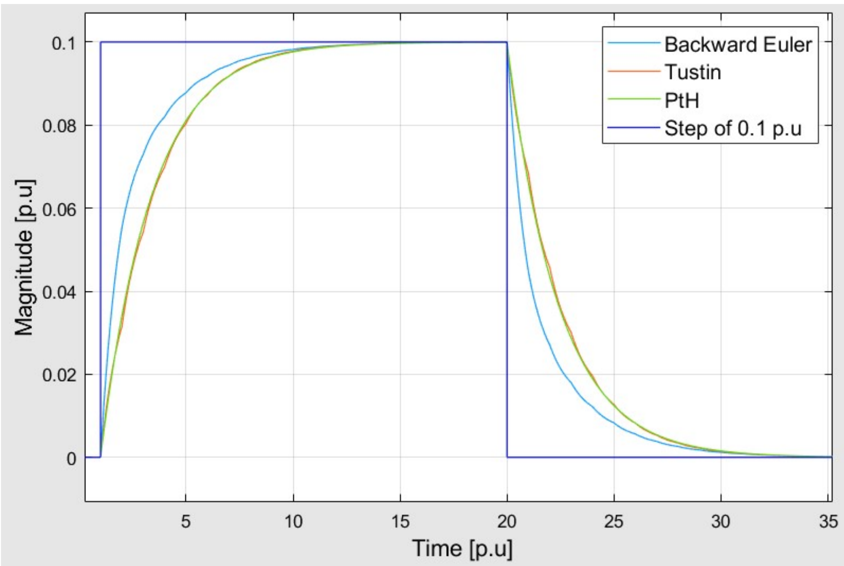

Figure 6.8: Comparison of the discretization methods Backward Euler and Tustin.

6.2 Test of constraint functions with discrete controller

In Figure 6.9 a test of a step up and down of 0.1 p.u is shown. The test is to verify the HPPs capability of stepping up and down according to the grid code. From the figure, it is seen that the HPP output is decreasing when a step down of 0.1 occur at 40 seconds. However, the power production from the PtH remains at 1 p.u and is not affected by the step. This is also seen at 60 seconds when the power output at PCC is increasing by a step of 0.1 p.u. The controller is ensuring that the reference at PCC is following the DSO reference, while the PtH plant is consuming maximum power.

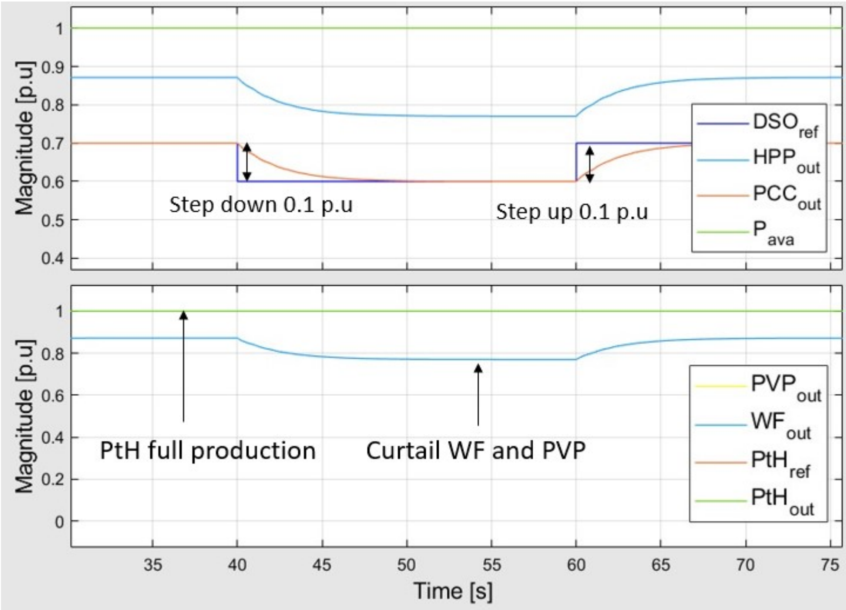

Figure 6.9: Step up/down of 0.1 p.u.

To test the discrete controller in different scenarios a ramping up/down of 0.00167 p.u/s with delta constraint is shown in Figure 6.10. At 50 seconds the power output at PCC starts to decrease by ramping down of 0.00167 p.u/s (100 kW/s). While the power output at PCC decreases, the PtH plant starts consuming excess power from the plant. This is seen from HPP that is producing more power than needed in PCC. Between 160-300 seconds the delta is shown and full utilization of the PtH is seen. At 300 seconds the power output at PCC starts to increase again and the PtH plant decreases to follow the reference from the DSO at PCC.

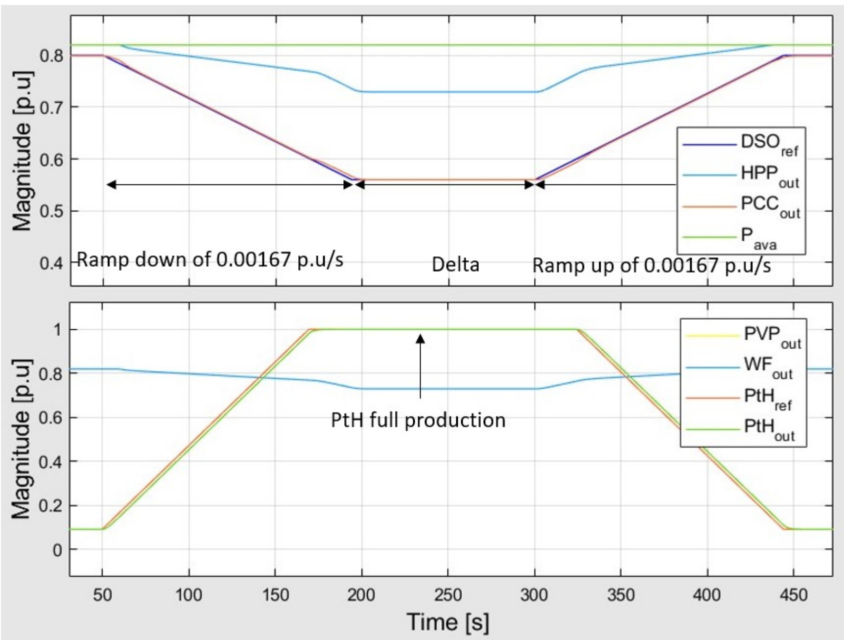

Figure 6.10: Delta constraint with ramp up/down of 0.00167 p.u/s

To ensure that the controller is able to down scale the power output at PCC in case of an increase in the grid frequency, a test of frequency response is shown in Figure 6.11. At 70 seconds the frequency exceeds F_R (50.2 Hz) and the power output at PCC decreases. However, when the power output at PCC decreases the power output from the HPP is sending the excess available power in the system to the PtH. This is seen in the figure and the PtH is ramping up and the power at PCC decreases. Furthermore, when the frequency decreases again the power output at PCC increases and the PtH is curtailed.

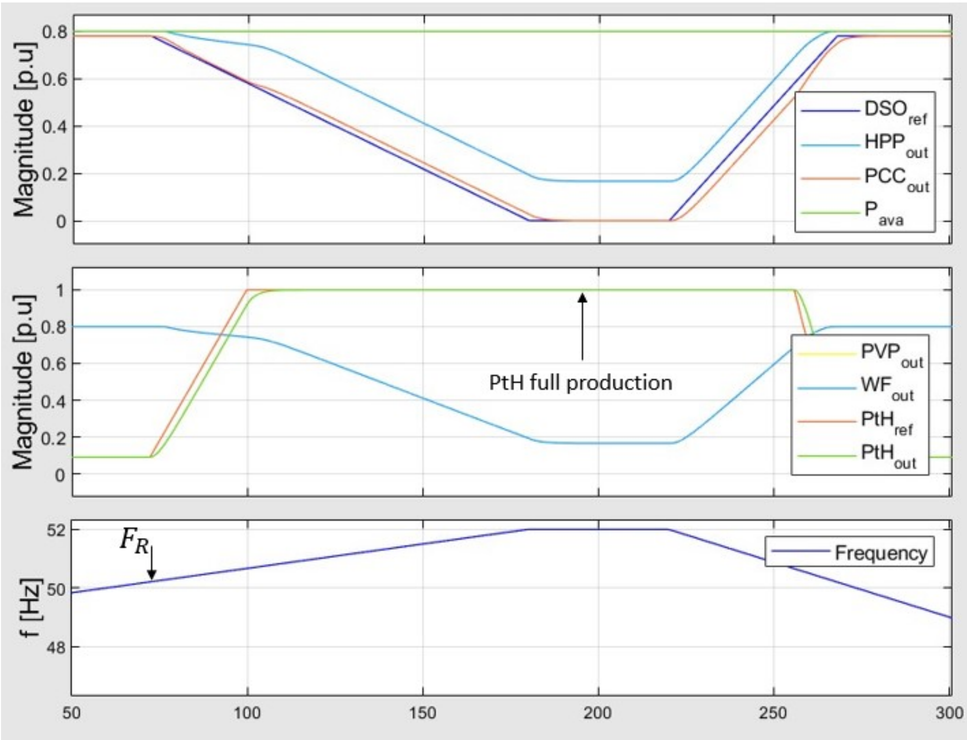

Figure 6.11: Frequency response.

In Figure 6.12 the ramping and power delta constraints are shown with maximum utilization of the wind turbines. The power output at PCC follows the reference setpoint while the excess available power is consumed in the PtH plant. At 50 seconds the setpoint is ramping down with 0.00167 p.u/s. It is seen that the WF power output is utilizing the available power, while the PVP is curtailing to follow the now setpoint for PCC. The power production from the HPP distributes excess available power to the PtH plant without affecting the power output at PCC.

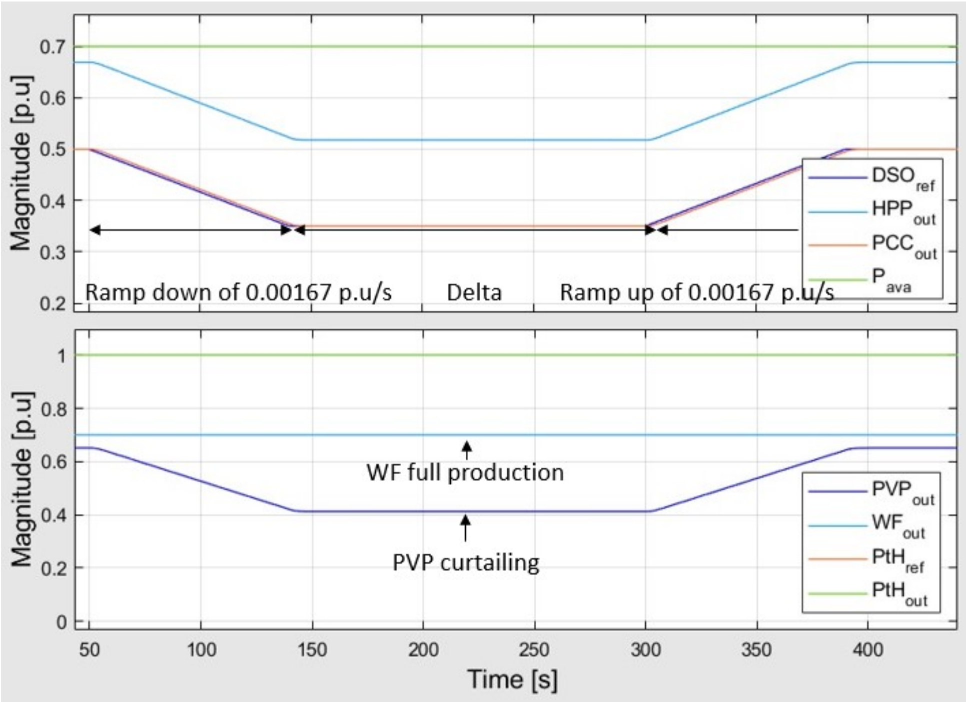

Figure 6.12: Delta power constraint with maximum utilization of the wind power.

6.3 Summary

In this section, different discretization methods for the controller have been investigated. It was seen that a sampling time of T_s= 1 s for the discrete was similar to the continuous controller. However, fine-tuning was needed in order to fulfill the requirements for the controller. For the discrete controller, the Tustin method has been chosen due to the step response was similar to the step response of the PtH plant. Furthermore, the constraint functions for the HPP were tested according to the grid codes. It is seen that the implemented discrete controller is able to fulfill the requirements.

7 Chapter 7: Conclusion

This chapter present the results obtained in this thesis. This includes discussion of the performance from the developed active power control and outlines of the future work is presented.

7.1 Conclusion

This thesis has presented the problems of combining renewable energy sources with a power to hydrogen plant to utilize surplus energy produced in the hybrid power plant. The main objective is to develop an active power control to comply with the grid codes for an HPP compound by a WF, PVP, and PtH.

The current background for developing a hybrid power plant including power to hydrogen is presented in the first chapter. The future of danish energy production is carried out by wind turbines with a combination of PtH or storage. This is also seen for already existing renewable power plants where additional implementation of storage is incorporated in the plant. Chapter 2 presented an overview of the current technologies in the market today. The state of the art of renewable park controllers has been presented. Moreover, several dispatch strategies have been investigated for power plant control and due to the complexity further development of this was needed.

A model of the proposed hybrid power plant is introduced in Chapter 3. The design of the power plant is based on an already existing plant located in the Netherlands rated 60 MW (38 MW PV and 22 MW WT). Based on literature for the PtH plant, a rated capacity of 10 MW was chosen for the system. The steady-state behavior of the system has been investigated to analyze the system under different operational conditions with varying SCR and XR ratios. It is seen that depending on the external grid parameters the losses in the system are lowered or increased. The system is also tested based on different voltage magnitudes in order to investigate the influence on the system based on the grid voltage. Furthermore, the influence of the power to hydrogen plant in the system has been tested with varying power consumption. It is seen that when the plant is consuming power from the WTs and the PVs, the losses in the system are lowered. Therefore, implementing the PtH does not cause any additional losses in the system. A simplification of the production units (wind turbines, PVs, and electrolysis) is obtained in order to apply classic SISO theory to the system. Based on the losses in the system two types of controllers have been developed and investigated. The design of the controllers is based on the danish grid codes. However, grid codes for an HPP do not exist and worst-case both WF and PVP grid codes are then chosen for the controller design. The P controller has been designed based on the steady-state error criteria. The results for the P controller shows that in order to comply with the steady-state error of 2 % of P_n a large overshoot is introduced to the system. Therefore, a P controller is not suitable for the HPP. A PI controller has been designed based on the Modulus Optimum method. It was seen that the PI controller is faster than the electrolysis plant and to avoid disturbances in the system, a pole-zero cancellation has been made. This results in a controller with a time constant matching the electrolysis plant time constant. The robustness of the controller has been verified based on different operational conditions. It was seen that for varying SCR, XR ratio, and different voltage magnitude the controller is able to comply with the grid codes. Based on steady-state conditions, the controller has been tested according to the functionalities of the grid codes. This includes active power constraint, delta constraint, ramp rate constraint, frequency response, and frequency control. During the test of the controller, different dispatch strategies have been tested. Due to the production profiles of the WF and PVP, a proportional dispatch has been chosen for the test. It is seen that the dispatch is distributing the power reference based on the available power from both the WF and PVP. To minimize the stress on the mechanical parts of the wind turbine a test has been carried out, where the WF is producing maximum power and the PVP is adjusting the power production to comply with the grid codes. From the test, it is seen that the controller is decreasing the PVP production without adding any disturbances to the power output at PCC. Throughout the tests, the utilization of the excess available power has been distributed to the PtH plant. It is seen that the requested power at PCC has not been affected by the operation of the PtH plant. Furthermore, it has been seen that the production from the PtH plant is curtailing when power is needed at PCC. This means that the HPP is able to utilize excess available power in the system without affecting the power output at PCC and still meet a settling time lower than 10 s. To implement the controller in real life, the effect of different discretization methods has been investigated. The transformation from the s domain to the z domain is made based on the pole-zero cancellation and it is seen that further fine-tuning is needed to comply with the grid codes. For the Backward Euler method, an increment of Kp was needed to comply with the grid codes of a settling time lower than 10 s. For the Tustin method, the Kp needs to be decreased to comply with the grid codes. By comparing the two methods with the PtH plant, the Tustin method has been chosen for implementation in the system. This is to avoid any disturbances when the HPP is operating. The discrete controller has then been tested in order to comply with the grid codes and functionalities needed for the system.

7.2 Future work

The purpose for the thesis has been to develop and implement a hybrid power plant including a power to hydrogen plant. This is to utilize the excess available power in the system to maximize the profit of the plant. This section explains the future work, which will be the following steps for development of the different methods to control and operate the plant.

- Implementation of the controller in Real-time evaluation of the model in a Hardware-in-the-loop test.
- Implementation of full scale renewable park controller including active power control and reactive power control and test the controller under fault conditions.
- Implantation of optimized dispatch strategy to reduce operational cost and maximize the power output of the plant.

References

[1] *Klimaaftale for energi og industri mv. 2020*, https://kefm.dk/Media/8/8/aftaletekst-klimaaftale-energi-og-industri%20(1).pdf, Last accessed on 07-02-2022.

[2] *Energiaftale 2018*, https://kefm.dk/media/6646/energiaftale2018.pdf, Last accessed on 07-02-2022.

[3] *Ptx in denmark before 2030*, https://energinet.dk/-/media/8BF0CD597E1A457C8E9711B50EC27 82A.PDF, Last accessed on 08-02-2022.

[4] *Energi ø - faktaark*, https://kefm.dk/Media/4/A/faktaark%20om%20Energi%C3%B8.pdf, Last accessed on 08-02-2022.

[5] *European energy på vej med kæmpe ptx-projekt i nordjylland*, https://www.energy-supply.dk/arti cle/view/827405/european_energy_pa_vej_med_kaempe_ptxprojekt_i_nordjylland, Last accessed on 09-02-2022.

[6] J. F. Alin Gerorge Raducu Nikolaos Styliaras and C. Ionita, "Design and implementation of a hybrid power plant controller," 2018.

[7] J. M. Garcia, "Voltage control in wind power plants with doubly fed generators," 2010.

[8] L. Petersen, F. Kryezi, F. Iov, Ł. H. Kocewiak, "Wind power plant control optimisation with incorporation of wind turbines and statcoms," 2015.

[9] L. Meegahapola, D. Flynn, "Impact on transient and frequency stability for a power system at very high wind penetration," 2010.

[10] L. Petersen, B. Hesselbæk, A. Martinez, R. Borsotti-Anderuszkiewicz, G. Tarnowski, N. Steggel, D. Osmond, "Vestas power plant solutions integrating wind, solar pv and energy storage," 2018.

[11] Energinet, "Teknisk regulering 3.2.5," 2019.

[12] ——, "Teknisk regulering 3.2.2," 2014.

[13] ——, "Teknisk regulering 3.2.1," 2017.

[14] ——, "Ancillary services to be delivered in denmark - tender conditions," 2021.

[15] *Hyprovide a-series*, https://greenhydrogen.dk/wp-content/uploads/2021/02/A-Series-brochure-1 20421.pdf, Last accessed on 07-04-2022.

[16] Anca D. Hansen, Poul Sørensen, Florin Iov, Frede Blaabjerg, "Centralised power control of wind farm with doubly fed induction generators,"

[17] D. Pombo, F. Iov, D. Stroe, "A novel control architecture for hybrid power plants to provide coordinated frequency reserves," 2019.

[18] Ignatius Rendroyoko, Ngapuli Irmea Sinisuka, Deddy P Koesrindartoto, "Optimizing unit commitment schemes for variable res power plant integration in microgrid systems,"

[19] C.-L. Chen, "Optimal wind–thermal generating unit commitment,"

[20] *Hybalance*, https://hybalance.eu/wp-content/uploads/2020/10/HyBalance_Brochure_Sep2020_Fin al.pdf, Last accessed on 11-04-2022.

[21] *Shell starts up europe's largest pem green hydrogen electrolyser*, https://refhyne.eu/shell-starts-up -europes-largest-pem-green-hydrogen-electrolyser/, Last accessed on 12-04-2022.

[22] *Vattenfall's largest hybrid energy park is taking shape in the netherland*, https://group.vattenfall.c om/press-and-media/newsroom/2020/vattenfalls-largest-hybrid-energy-park-is-taking-shape-in-t he-netherlands, Last accessed on 15-05-2022.

[23] T. N. Preda, K. Uhlen, D. E. Nordgård, T. Toftevaag, "External grid representation for assessing fault ride through capabilities of distributed generation units,"

[24] Torben Knudsen, Thomas bak, Mikael Svenstrup, "Survey of wind farm control, power and fatigue optimization,"

[25] Lennart Petersen , Florin Iov , Anca Daniela Hansen , Mufit Altin, "Voltage control support and coordination between renewable generation plants in mv distribution systems," 2016.

[26] L. Petersen, F. Iov, G. C. Tarnowski, V. Gevorgian, P. Koralewicz, D. Stroe, "Validating performance models for hybrid powerplant control assessment," 2019.

[27] Andrés Honrubia-Escribano, Francisco Jiménez-Buendía, Emilio Gómez-Lázaro, Jens Fortmann, "Validation of generic models for variable speed operation wind turbines following the recent guidelines issued by iec 61400-27," 2016.

[28] Abbas Seif, Shahram Karimi, Hamdi Abdi, Mehrdad Fazli, "Comparison of dfig and sef-dfig operation in wind turbine systems," 2015.

[29] Vestas, *General Specificatio, V112–3.0 MW 50/60 Hz*. Vestas wind system A/S, 2010.

[30] L. Petersen, "Proof-of-concept on next generation hybrid power plant control," 2020.

[31] F. Alhuwaishel, A. Allehyani, S. Al-Obaidi, P. Enjeti, "A new medium voltage dc collection grid for large scale pv power plants with sic devices," 2018.

[32] R. Machlev, Z. Batushansky, S. Soni, Y. Levron, J. Belikov, V. Chadliev, "Verification of utility-scale solar photovoltaic plant models for dynamic studies of transmission networks," 2020.

[33] M. Kopp, D. Coleman, C. Stiller, K. Scheffer, J. Aichinger, B. Scheppat, "Energiepark mainz: Technical and economic analysis of the worldwide largest power-to-gas plant with pem electrolysis,"

[34] I. renewable energy agency, "Green hydrogen cost reduction," 2020.

[35] H. Saadat, *Power system analysis*. Psa Publishing, 2010, ISBN 9780984543861.

[36] J. Duncan, Thomas J Overbyw and Mulukutla S. Sarma, *Power system analysis and design*.

[37] G. R. C. Mouli, P. Bauer, T. Wijekoon, A. Panosyan, E. Baerthlein, "Design of a power electronic assisted oltcfor grid voltage regulation," 2014.

[38] N. S. Nise, *Nise's control system engineering*. Markono Print Media Pte Ltd, 2015, ISBN 978-1-119-38297-3.

[39] J. M. Garcia, "Voltage control in wind power plants with doubly fed generators," 2010.

[40] M. Comanescu, "Influence of the discretization method on the integration accuracy of observers with continuous feedback," 2011.